



NTNU – Trondheim
Norwegian University of
Science and Technology

Micro-fluidic flow cells for studies of electrochemical reactions

Mats Ingdal

Materials Technology

Submission date: July 2014

Supervisor: Frode Seland, IMTE

Co-supervisor: Svein Sunde, IMTE

David A. Harrington, University of Victoria

Norwegian University of Science and Technology
Department of Materials Science and Engineering

Preface

This work has been performed as a part of the master program “Material Chemistry and Energy Technology” at Norwegian University of Science and Technology (NTNU) in the spring of 2014. The project is a collaboration between NTNU and the University of Victoria (UVic) and the majority of the work was performed at UVic. This work is a part of a large NTNU research project: “Microfluidic flow cell in the service of fuel cell electrocatalysis”.

I would like to thank my supervisors for help and constructive feedback throughout the entire duration of this project. In particular I would like to thank my supervisor in UVic, David Harrington for welcoming me to Canada, supplying necessary equipment and chemical and providing valuable input. I would also like to thank my co- supervisor Thomas Holm whom been the perfect research partner during my lab-work.

I declare that the work has been performed independently and in accordance with the rules and regulations of the Norwegian University of Science and Technology.

Mats Ingdal

Trondheim 28.07.2014

Abstract

Micro fluidic flow cells (MFFCs) are a relatively new technique for characterization of electrochemical reactions. This work includes both techniques for manufacturing the cells and electrochemical characterization of them.

Improvements to a previously established procedure for the manufacturing MFFCs included change of template for PDMS-masters from glass slides to silicon wafers and the change from electrodes consisting of titanium gold and platinum to only titanium and platinum. The changes to the PDMS-masters improved the channel parameters and durability. The changes to the electrodes removed the problem with exposed gold surfaces interfering with at the platinum electrode, and increased the lifetime of the electrodes significantly. A method for removing oxygen from the MFFCs was also established.

Experiments using ferrocyanide redox couple did not show reversible behavior using both platinum and iodine-coated platinum electrodes. Experiments using ruthenium redox couple achieved near reversible behavior using both platinum and iodine-coated platinum electrodes. The iodine-coating showed higher stability and was implemented as a part of the standard procedure.

The effect of the placement of the internal reference electrode was investigated. The results indicate that the reference should be place upstream for the working electrode and the counter electrode should be placed downstream for the working electrode. The distance between the working and counter should exceed the distance between the working and reference electrode to minimize interference.

Results from potentiostatic and downstream galvanostatic electrochemical impedance both showed trends compatible with theoretical predictions. Due to fluctuations in the open-circuit potential the results showed low reproducibility.

Sammendrag

Mikrofluidiske-strømningsceller er en relativt ny metode som benyttes for å karakterisere elektrokjemiske reaksjoner. Dette arbeidet inneholder teknikker for fabrikking og elektrokjemisk karakterisering av slike celler.

Tidligere etablerte prosedyrer for fabrikking av mikrofluidiske-strømningsceller ble forbedret på to punkter. Grunnplata for bygging av "PDMS-masters" ble endret fra glassplate til siliko wafer. Denne endringen forbedret både kanalparametrene og levetiden. Sammensetningen av elektrodene ble også endret fra trelags elektroder sammensatt av titan, gull og platina til kun titan og platina. Endringen førte til en signifikant økning i levetiden til elektrodene og fjernet problemet med eksponert gulloverflate som blandet seg med elektrodens platinaoverflate. En metode for å fjerne uønsket oksygen fra strømmingcellene ble også utviklet.

Elektrokjemiske forsøk som benyttet ferrocyanid redokspar oppnådde ikke reversible oppførsel for både platina og jod-dekte platina elektroder. Forsøk som benyttet ruthenium redokspar oppnådde nær reversibel oppførsel for både platina og jod-dekte platina elektroder. Effekten av jodlaget var høyere stabilitet og ble implementert som en del av en standardisert prosedyre.

Effekten av plassering av referanse-elektroden ble undersøkt. Resultatene indikerte at referanse-elektroden bør plasseres oppstrøms for arbeids-elektroden og mot-elektroden bør plasseres nedstrøms for arbeids-elektroden. Videre bør avstanden mellom arbeids- og mot-elektroden overstige avstanden mellom arbeids- og referanse-elektroden for å minimere påvirkningen på referanse-elektroden.

Resultater fra potensiostatisk- og nedstrøms- galvanostatisk -elektrokjemisk impedans viste trender som er forenlige i litteraturen. Grunnet ustabil åpen-krets-potensial ga resultatene lav reproduserbarhet.

Contents

Preface.....	i
Abstract	ii
Sammendrag	iii
1. Introduction.....	1
2 Theory.....	4
2.1 Microfluidic flow-cells.....	4
2.1.1 Electrochemical detection devices.....	4
2.1.2 Microfluidic fuel cells.....	6
2.2 Electrochemical methods.....	10
2.2.1 Cyclic voltammetry.....	10
2.2.2 Impedance spectroscopy.....	14
2.2.3 Ferricyanide/ferrocyanide couple.....	16
2.2.4 Ruthenium hexamine (II/III) redox couple.....	16
2.2.5 Iodine film.....	17
2.3 Production methods.....	18
2.3.1 Photolithography.....	18
2.2.2 Metal deposition.....	19
2.3.3 PDMS.....	19
3 Experimental.....	20
3.1 Production of MFFC.....	20
3.2 Electrochemical experiments.....	24
4. Results and Discussion.....	27
4.1 Redesign of PDMS masters.....	27
4.2 Gold-platinum electrode characteristics.....	29
4.3 Oxygen elimination and proper voltammetric baseline response with a custom-made environmental chamber.....	33
4.4 The ferricyanide/ferrocyanide redox couple.....	37
4.5 The ruthenium redox couple.....	39
4.6 Deposition and stability of the iodine layer.....	41
4.7 Positioning of the reference electrode and resistance measurements in MFFCs.....	45
4.8 Potentiostatic electrochemical impedance.....	53

4.9 Downstream galvanostatic electrochemical impedance	55
5. Conclusion	58
6. Further work	60
7. References	61
Appendix A	62
Detailed step-by-step procedure for production of MFFCs.	62

1. Introduction

The transition from a society based on non-renewable to a renewable energy sources involves several technological challenges. One of proposed energy carriers of the future is hydrogen. Hydrogen and oxygen can be efficiently converted to water and electricity using a fuel cell. The use of hydrogen has several challenges that need to be addressed; the need for a CO₂ neutral production of hydrogen, an extensive infrastructure for storage and distribution, and improvements to today's technology for end use of hydrogen. Liquid hydrogen carriers such as ethanol, methanol and formic can be utilized in fuel cell devices. These organic fuels can take advantage of the existing infrastructure are available both from the fossil reserves and from renewable biological sources, they are liquid at operation and storage temperature, they have high energy density and can be stored more efficiently than hydrogen making them a potential fuel for the transition towards a sustainable energy society [1].

One of the alternatives for liquid biofuels is the PEM fuel cell. However the direct oxidation of these fuels is complicated and leads to high anodic over-potentials. Empirical studies have made improvements to the electrocatalysts but the understanding of the mechanism has lagged behind. A better understanding of the kinetics and electrochemical pathways of such fuels can help the development of electrocatalysts and is necessary for development and improvement of fuel cells employing liquid biofuels [1].

The overall aim of this project is to employ a relatively new technique using microfluidic flow cells (MFFC) as primary detection device to increase the understanding of the reactions and their kinetics[1].The characteristics of microfluidic flow cells can prove beneficial to the study of electrochemical reactions. The laminar flow characteristics of the microfluidic devices allows for a better control of the mass transport compared to traditional electrochemical characterization techniques such as rotating disc electrode

and wall jet electrode [2], and these flexible production methods of the cells allows for multiple electrode designs [3].

Microfluidic devices constitute a large and important field of research. The span of the research stretches from capillary electrophoresis, electrochemical detection [4], to fuel cell devices [5, 6]. The constant improvement of micro-fabrication techniques has driven the development of so-called lab-on-chip devices over the last decade. The development of the fabrication methods has allowed for cheap, efficient and flexible designs of such devices [4].

Electrochemical detection using microfluidic devices is considered to have a wide range of applications including biological research, real-time detection, monitoring of biological threats and disease diagnosis in point-of-care medical tests. Such devices offer a simplification of complex analyses, portability, disposability and reduction in cost [7]. These kind of devices also have the possibility of multiple electrode configuration that can help minimize interference and increase sensitivity [3].

The increase in energy demand for portable devices has prompted the need for power supplies with higher energy densities. One of the most promising candidates for this purpose is the microfluidic fuel cell. The microfluidic fuel cell utilizes fuel with a higher energy density than batteries and removes the need for a gas storage tank and a membrane required by the hydrogen fuel cell. In the micro channel of the microfluidic fuel cell there is a laminar flow regime between two liquids. This regime can be used to prevent the two different phases from mixing and prevent the need for a membrane to separate the phases [5, 6].

Work that has included electrochemical characterization using microfluidic devices is limited. Examples include work by Gutz [3] and Kjeang [8]. Gutz published in 2005 a study on microfluidic cells with integrated array of gold electrodes including fabrication and electrochemical characterization [3]. Kjeang's work included the electrochemical

velocimetry for a reversible redox species using a microfluidic device containing three gold electrodes [8].

The aim of this work is to further develop a manufacturing procedure for producing functioning MFFCs of a high quality and to establish the foundation for the study of electrochemical reaction in these MFFCs. The main body of the work consists of establishing techniques necessary for electrochemical characterization of the MFFCs using a highly reversible redox couple and known chemical techniques, as cyclic voltammetry and electrochemical impedance. The work consists of a small literature study that gives a short introduction to the properties, uses and characteristics of microfluidic devices, an introduction to the electrochemical methods employed and an introduction to the production methods used to fabricate the microfluidic flow cells and a large experimental section.

2 Theory

2.1 Microfluidic flow-cells

Microfluidic devices are today an important and large research field. There are several different types of devices that use the advantages of the microfluidic properties and miniaturization. These types of devices are often referred to as lab-on-chips and use the technology developed by the microelectronic industry to produce the devices [4]. The microfluidic devices can be categorized into three different categories; capillary electrophoreses devices, devices for electrochemical detection and microfluidic fuel cells [5]. Capillary electrophoreses devices are not included in the scope of this project and will not be discussed further.

2.1.1 Electrochemical detection devices

The development of microfluidic devices for electrochemical detection has been driven by several factors. The miniaturization of the detection device allows for smaller chemical assays and reduces both the sample and reagent size. The use of electrochemical detectors in micro channels results in low detection limits, and the constant development of fabrication-techniques reduce the cost and improve the quality. Another advantage of using these techniques is that they allow dual or multiple sensors to be placed in one channel. The multiple electrodes can help increase sensitivity of the analyses, removing interfering species or generating electrochemical active species [3]. Figure 1 shows an example of multi electrode flow cell device containing 20 gold electrodes in a PDMS channel [4].

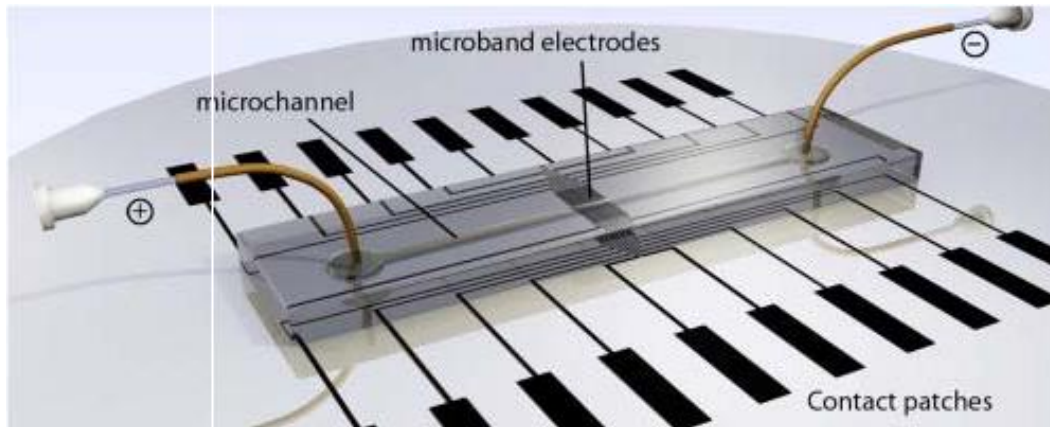


Figure 1. Schematic overview of a multi electrode flow cell device containing 20 gold electrodes in a PDMS channel [4].

This type of detector also has an advantage compared to other hydrodynamic approaches such as rotating disc electrode and wall-jet electrode, it allows for the possibility of better control over the mass transport through manipulation of the flow rate over a wider range [2].

Other uses for the dual micro band electrodes have been in electrochemical titration. The titration system consists of a generator and a collector electrode. The generator is situated upstream for the collector. At the generator an electrochemically active substance is produced. This product reacts with the solution and at the collector either the active substance or its reaction products are detected. This method can be used as a simple and inexpensive method for endpoint detection [9, 10].

Collection efficiency in this report is defined based on a dual-electrode system. The system consists of two working electrodes where the potential of each electrode can be controlled independent of each other. Working electrode is the generator and is placed upstream of the collector electrode. At the generator a product is produced by the means of an electrochemical reaction. This product is then detected by the second working electrode, the collector. The collection efficiency (CE) is then defined as the ratio between the current detected (i_c) by the collector and the current used to generate the product at the generator (i_g) as shown in Equation 1 [11, 12].

$$CE = \frac{i_c}{i_g} \quad [1]$$

There are many different methods used for determining collection efficiency. Two of the most common are the rotating ring-disc electrode and the channel flow double electrode. At the rotating ring-disc electrode the product is generated at the disc electrode, and then swept outwards towards the ring due to the radial flow. The product is then detected at the ring and the collection efficiency can be calculated.

The channel flow double electrode consists of a thin rectangular channel that passes over two working electrodes where the upstream electrode is the generator and the downstream electrode is the collector [11].

2.1.2 Microfluidic fuel cells

Microfluidic fuel cells or laminar flow-based fuel cells are described as a promising alternative to batteries for future portable electronic devices. Kjeang defines a microfluidic fuel cell as “a fuel cell with fluid delivery and removal, reaction sites and electrode structures all confined to a microfluidic channel” [5]. The microfluidic fuel cell has many of the same advantages as other electrochemical energy conversion devices; they operate at low temperature, have no moveable parts and can be made by simple techniques. Microfluidic fuel cells have a theoretical capacity for a higher energy density than batteries due to the nature of the fuel used. This, together with the technological-based prediction that batteries cannot “keep up” with increasing power demands of portable electronic devices, makes micro fluid fuel cells a promising alternative for the future [6].

An important feature of the microfluidic fuel cell is the laminar flow of the fluids inside the micro channel. This allows for two or more co-laminar flows to be present within the fuel cell without mixing and therefore removes the need for a membrane. For fuel cells it is common to use two different fluids, an anolyte and a catholyte or more commonly

referred to as the fuel and the oxidant. Using a different channel designs the two different fluids can be introduced in to the fuel cell without prior mixing [5]. An example of such design is the “Y”-design employed by Kjeangs high-performance microfluidic vanadium redox fuel cell. A schematic drawing of this design is shown in Figure 2 [13]. In the absences of a chemical reaction and electron migration between the two different laminar flows, mixing will be due to transverse diffusion. Due to the relative speed of the diffusion compared to the flow of reactants the diffusive mixing will be restricted to a thin hour-glass shaped layer in the middle of the channel. Another advantage of the co-laminar behavior is that the supporting electrolyte of each reacting specie can be chosen independent of each other. The individual electrolytes can be chosen to optimize reaction rates and cell voltage. Electrochemical reaction takes place on the surface of the electrode and miniaturization of the channel further improves the ratio between electrode surface and volume. However a reduction in the hydraulic diameter will increase the pressure drop within the micro channel and increase the necessary output of the pump to drive the fluid at a constant speed [5].

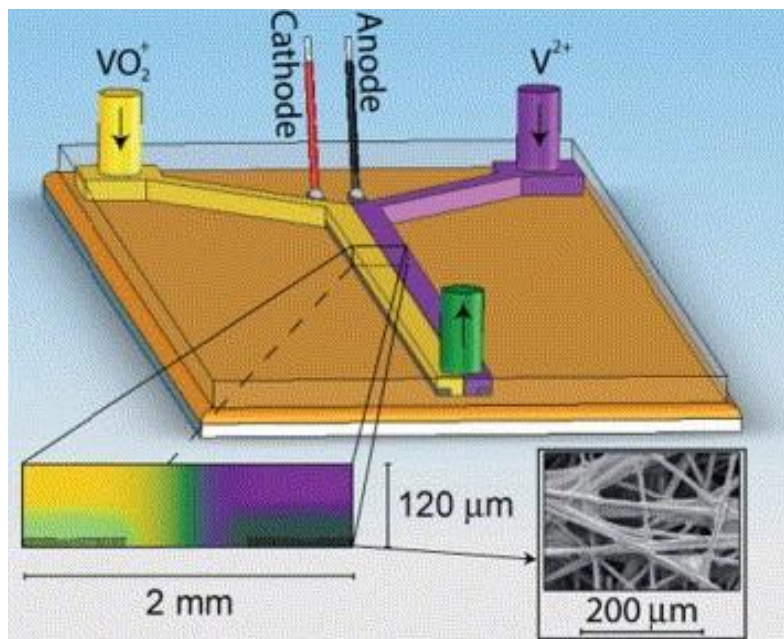


Figure 2. Schematic overview of a microfluidic fuel cell for vanadium redox complex illustrating the distribution of fuel (V^{2+} :purple) and oxidant (VO^{2+} :purple) in the micro channel. Small picture shows the porous carbon electrodes used in the fuel cell [13].

The microfluidic fuel cell follows the same principle as normal fuel cells. The main difference is that the membrane barrier between the two different compartments is replaced by a liquid-liquid interface barrier. The current collectors and electrodes are fabricated on the channel walls where the electrochemical reaction should take place. In order to complete the circuit the supporting electrolyte of both the fuel and the oxidant must have sufficient ionic conductivity. The driving force for the reaction can be estimated by the open circuit potential using the Nernst equation. The real potential is affected by activation, ohmic and mass-transport losses all causing a reduction of the effective driving force. When the electrochemical reaction takes place at the electrode surface both fuel and oxidant are consumed. The current density due to the reactions can be estimated using the Butler-Volmer equation. The current density is dependent on the replenishing rate of reactants to the surface. This rate is controlled by the flow rate in the channel leading to an increase of the cell's power output for high flow rate. However the increase in flow rate reduces the fuel utilization [6]. This effect is demonstrated by Kjeang's high-performance microfluidic vanadium redox fuel cell as shown in Figure 3. This work clearly shows the fall in fuel utilization as a function of flow rate, and the increase of power density with increasing flow-rate [13].

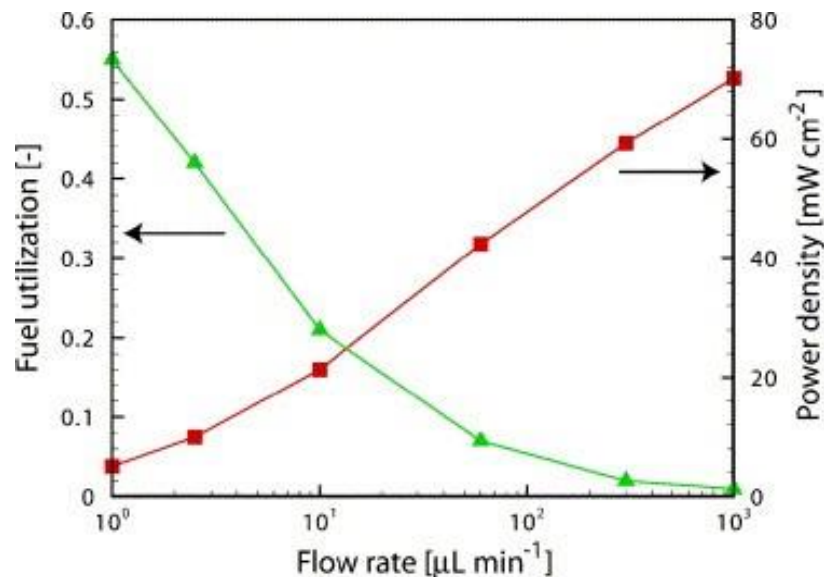


Figure 3. Performance data for high-performance microfluidic vanadium redox fuel cell. Green line indicates maximum fuel utilization per single pass. Red line indicates peak power density. (Both data were collected at room temperature as a function of flow rate) [13].

Kjeangs work [8] on integrated electrochemical velocimetry for microfluidic devices, describes two different flow regimes and their scaling laws for mass transfer controlled reactions. The two regimes are described by the dimensionless velocity parameter U^* . The high U^* regime is defined by high velocity, large hydraulic diameter and small width of the working electrode. The low U^* regime defined by low velocity, small hydraulic diameter and large width of the working electrode. The scaling laws for the high U^* are derived using a further simplification of the mass transfer model and results in the total current to be proportional to the cube root of the mean velocity. For the low U^* regime the assumption is that all reactants are consumed at the working electrode and the current then becomes proportional to the mean flow velocity [8].

Shaeng et al. describes the important performance parameters and the effect of different mechanisms on the performance of a membraneless laminar flow fuel cell using a concept map. This concept map gives a good overview of the determining factors and their effect for such fuel cells, and is presented in Figure 4 [6].

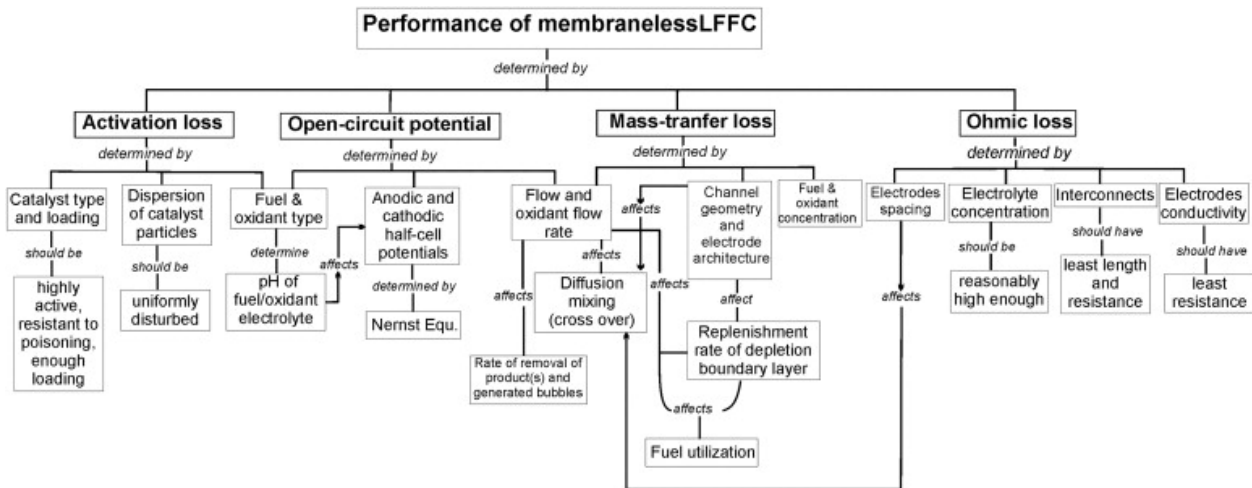


Figure 4. Concept map for important parameters concerning membraneless laminar flow-based fuel cells [6].

2.2 Electrochemical methods

2.2.1 Cyclic voltammetry

Cyclic voltammetry is a quasi-stationary electrochemical method. The principle behind the method is that the voltage is cycled in a triangular waveform while the current is measured. The triangular wave is shown in Figure 5. To generate this wave a potentiostat is used. For aqueous solutions the upper and lower potential limits are usually placed within the boundaries of hydrogen and oxygen evolution. The method gives high reproducibility of current-voltage behaviors for noble metals [17].

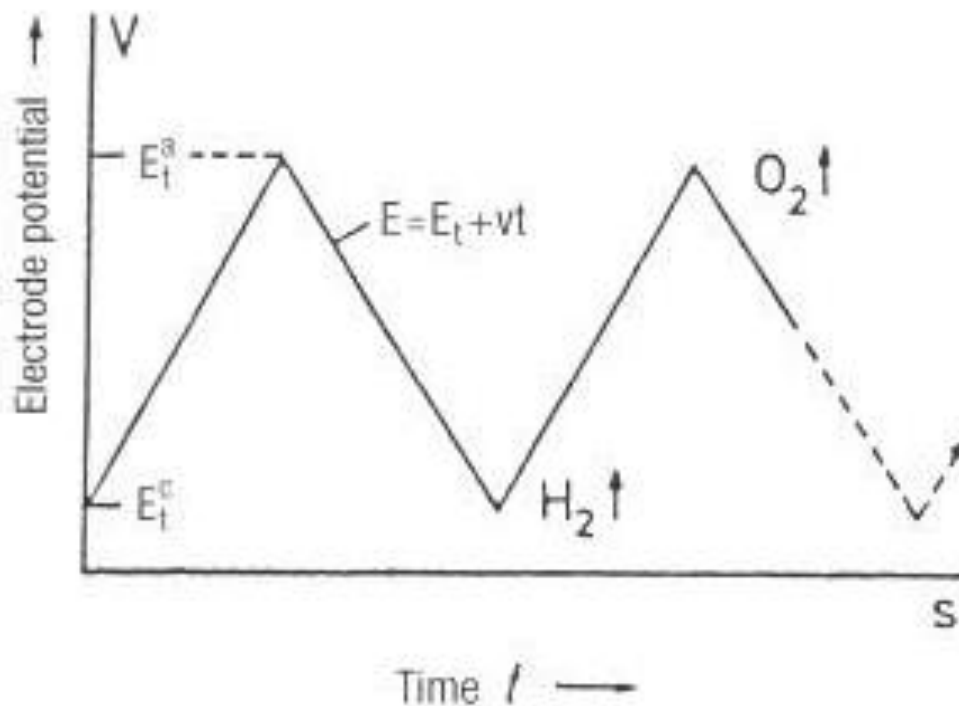


Figure 5. Potential-behavior for the working electrode as a function of time for cyclic voltammetry, where v is the sweep rate, t is time and E_c and E_{ta} is the cathodic and anodic turning potentials [17].

Data from cyclic voltammetry can be presented using a cyclic voltammogram. The cyclic voltammogram has the current density on the vertical axis and potential on the horizontal axis. Figure 6 and Figure 7 are examples of such cyclic voltammogram with only surface processes and with a bulk electrochemical reaction [17].

Cyclic voltammetry can be performed with only surface processes or with a bulk electrochemical reaction. The current-voltage behavior for platinum in an aqueous solution is an example of such a surface process. The peak in the cyclic voltammogram corresponds to dissolution and formations of chemisorbed oxide and hydride layers on the surface of the electrode and charging of the double layer. Figure 6 shows an example of such a voltammogram including the surface processes and evolution of oxygen and hydrogen in an aqueous 1M KOH electrolyte [17].

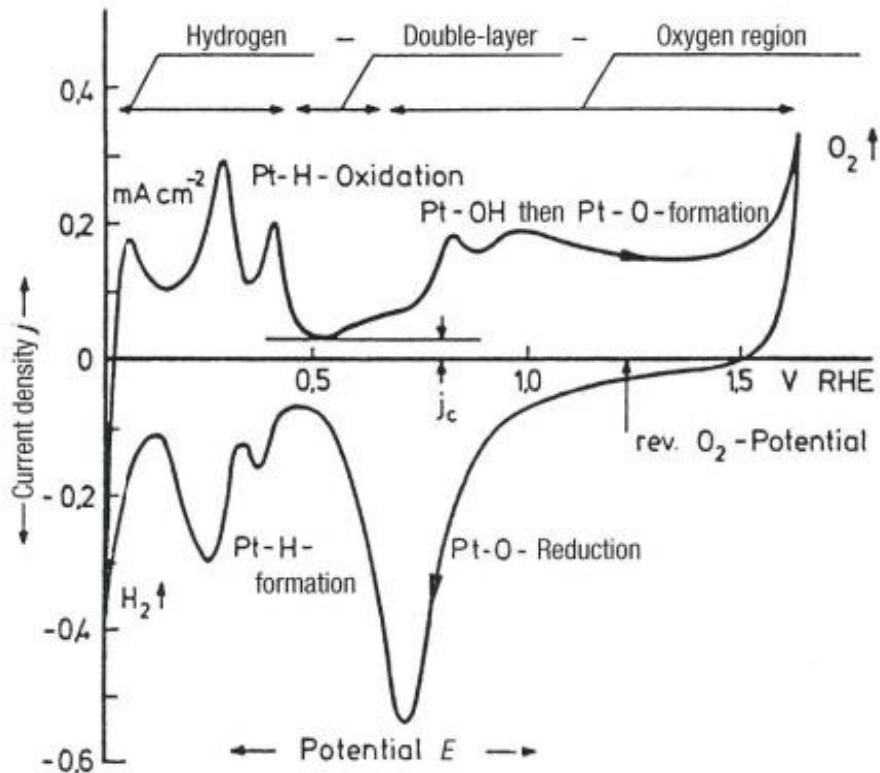


Figure 6. Cyclic voltammogram for platinum with only surface processes in a 1M KOH electrolyte. The data is collected at 20 °C in an N₂ purged electrolyte with a sweep rate of 100mV/s [17].

For cyclic voltammetry with an electrochemically active substance the chemical reaction will usually dominate the cyclic voltammogram in the areas where it is active. Initially the current is limited by a coupling of electron transfer and diffusion. As the potential sweeps, the over-potential of the reaction and the current increases and the surface concentration decreases until it reaches zero. At this point the reaction speed is no longer determined by the electron transfer, but is purely diffusion controlled. This point is defined as the limiting current. Increasing, the over-potential further after limiting current is reached will not increase the current. The current will rather fall with time until it reaches steady state at a finite diffusion layer thickness. For a complete cycle of a typical reversible redox couple starting at the open circuit potential and sweeping first in the anodic direction, a current due to oxidation of the redox species will occur according to the chemical reaction 2 [17].



During the subsequent negative going of the potential scan, a reduction current will occur due to the reduction of the earlier oxidized species according to Chemical reaction 3 [17].



An example of a cyclic voltammogram containing the previously mentioned typical reversible redox couple is shown in Figure 7 [17].

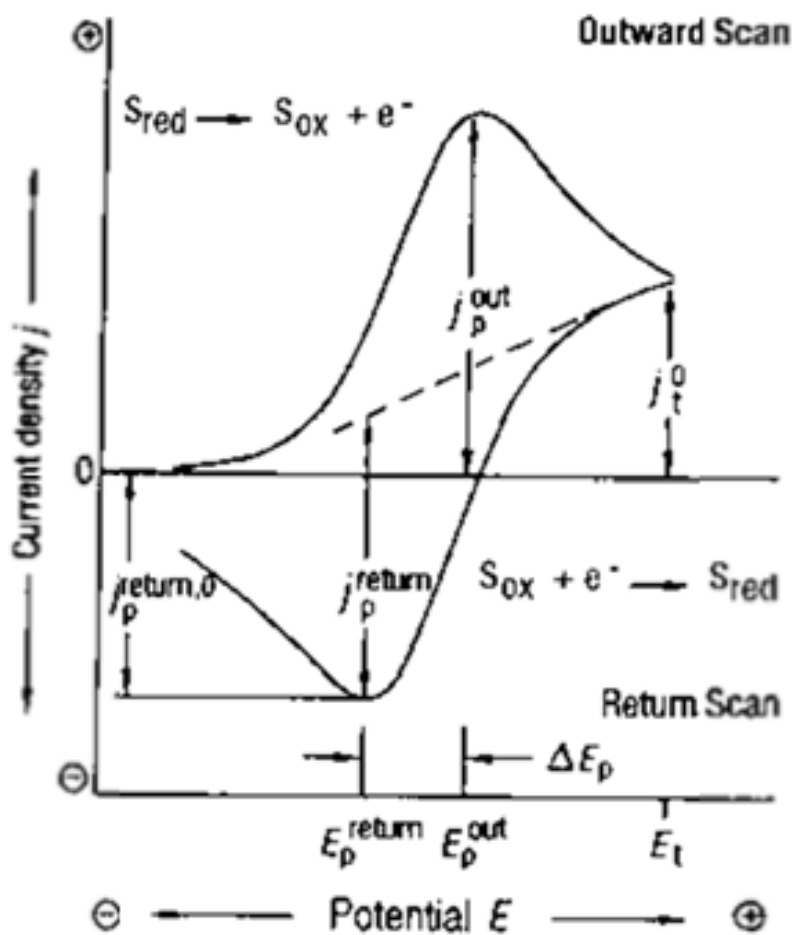


Figure 7. Illustration of cyclic voltammogram for a reversible redox system in a stationary solution containing data for one cycle [17].

When evaluating reactions for cyclic voltammetry it is normal to split them into two regimes, reversible and irreversible. For a reversible reaction it is assumed that electron transfer is so fast that the Nernst equation is fulfilled at the electrode surface at all times. The peak current location on the horizontal axis then becomes independent of sweep rate. Furthermore the ratio between the anodic and cathodic current becomes a function solely dependent on the turnaround potential (E_t). For an irreversible reaction the peak current is a result of both slow electron transfer and diffusion and is no longer independent of sweep rate. The peak current will shift to higher potentials as a function of higher sweep rates [17].

2.2.2 Impedance spectroscopy

Electrochemical impedance spectroscopy uses the combination of a small AC. sine wave and a DC. potential. This gives rise to a current response from the electrochemical system contain an AC. component whose phase that can be separated from the total signal through a sine wave detector. The phase and the magnitude are treated using the complex numbers, and the ratio between potential (E) and the current response (j) gives the impedance (Z), as shown in Equation 2 [18].

$$Z = \frac{E}{j} \quad [2]$$

Impedance spectroscopy is used to derive kinetic parameters from an electrochemical system. The electrochemical system consists of several different processes that respond differently to change in frequency. At low frequencies all processes are able to respond, as the frequency raises the response of some processes changes and this results in lower amplitude and increasing phase shift. When the frequency reaches a certain level specific to that process the process cease to respond. By scanning the system at different frequencies the kinetic behavior of the whole system can be mapped out [18].

A common way to interpret results from impedance spectroscopy is to consider an equivalent circuit consisting of known electrical components. Depending on the complexity of the system being studied, different components must be added.

Reactions can be controlled by electron transfer, diffusion or a combination of the two. Impedance spectroscopy allows the two different components to be separated. At high frequencies the reaction is controlled by electron transfer and this in combination with the double layer capacitance gives a characteristic semi-circle. At lower frequencies the reaction is controlled by diffusion, which gives a straight line known as the Warburg-line. Figure 8 shows a schematic of an electrode interface with a suggested equivalent circuit for a half-cell [18].

Figure 9 shows the Nyquist-plot resulting from such a circuit. Using extrapolation of the Warburg-line, it is possible to estimate the real contributions from the different sources to the impedance as shown in the Figure 8, where R_E is the resistance in the electrolyte, R_N is Nernst resistance and R_{CT} is the resistance to charge transfer [18].

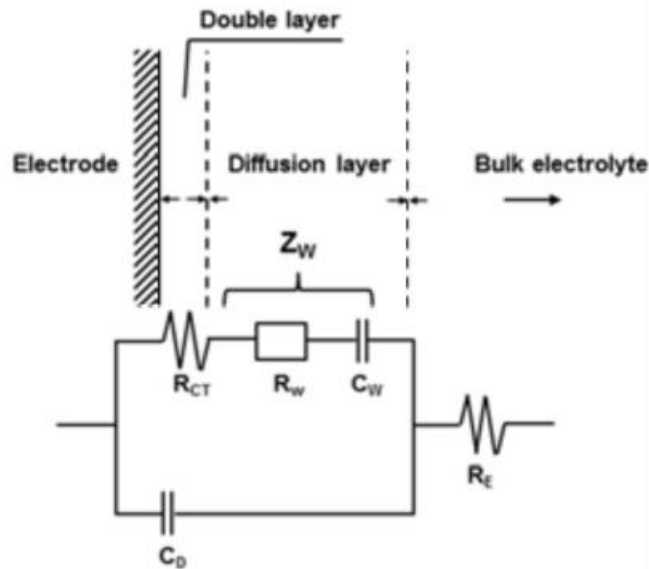


Figure 8. Equivalent circuit for a simple electrochemical system [18].

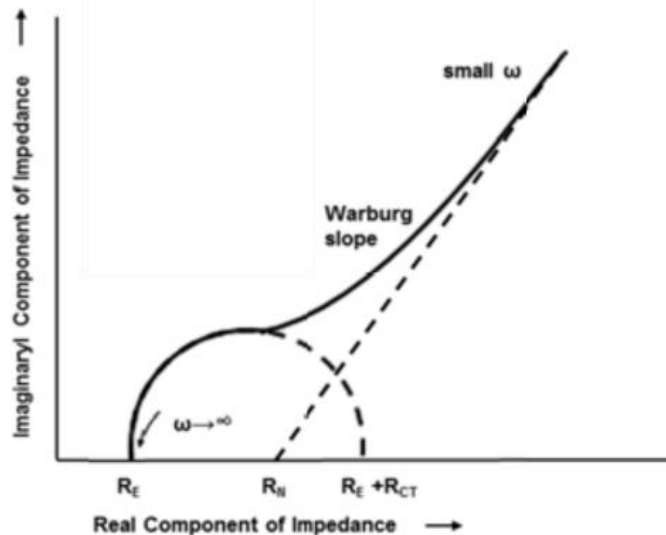


Figure 9. Corresponding Nyquist-plot for the system where the effect of diffusion and electron-transfer resistance is taken into account [18].

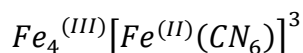
2.2.3 Ferricyanide/ferrocyanide couple

Ferricyanide/ferrocyanide extensively studied fast redox couple. It has been used as a model for fast simple redox reactions assuming simple outer-sphere electron transfer reaction. Chemical equation 3, show this simple redox reaction for the ferrocyanide redox couple [16, 17, 18].



Various studies have indicated that this process is in fact quite complex. Reported rate constants have shown dependence on the concentration of different cations and anions in the supporting electrolyte, and material and pretreatment of electrodes. Deactivation of the electrodes over time was also observed. The deactivation was explained by insoluble species, originating from the ferrocyanide couple, depositing on the surface and partial blocking it inhibiting electron transferee [16, 17].

Prussian blue is a pigment insoluble in water with the chemical formula:



Prussian blue has been used to modify platinum and gold electrodes. The electrodes were immersed in ferric-ferrocyanide solution to deposit a thin-film of Prussian blue. The mechanisms behind the deposition is thought to be auto- or catalytic- reduction. This deposition process has been found to be highly dependent on both chemical composition and substrate surface [18].

2.2.4 Ruthenium hexamine (II/III) redox couple

Ruthenium hexamine (II/III) is a commonly used highly reversible redox couple. This redox couple has often been used as a model for fast simple redox reactions in characterization of electrochemical systems. Chemical equation 4 shows the simple redox reaction. Reported standard rate constant for the redox couple are between 0.36 to 0.54 cm s⁻¹ [19, 20].



2.2.5 Iodine film

The interactions of halogens with metal surfaces have been extensively studied. This includes the interaction between I₂ and Pt. Iodine is known to adsorb at the platinum surface according to Chemical reaction 5 [21, 22, 23, 24].



The iodine film creates an unreactive protective layer that permits electron transfer, and was used to permit model behavior of the ferricyanide/ferrocyanide system [17].

Iodine can desorb from the platinum surface. The suggested reaction in acidic solution is shown in Chemical reaction 6 [22].



Thomas [22] showed that the degradation of the iodine layer due to desorption and diffusion processes for a fully covered platinum surface in the time span of 12h was 6%. However, for a half iodine-covered electrode exposed to the same treatment the degradation was 6 times higher. Further results indicate that allowing the iodine layer to interface with a clean Pt surface, increases the rate of the degradation process [22].

2.3 Production methods

The production methods used for manufacturing MFFC are methods developed primarily for the integrated circuit industry over the last 50 years. The literature therefore reflects this, but many of the same requirements necessary to create high quality integrated circuits are valid for the production of MFFCs.

2.3.1 Photolithography

Photolithography is a technique that is used to transfer a three-dimensional pattern to a surface using a light sensitive chemical, photoresist, and a controlled exposure of light. Photolithography is often considered the most critical step in the integrated circuit manufacturing and is the center of this process. The patterns created with photolithography is the starting point for many important processes in the integrated circuit manufacturing including; deposition of thin film, doping, etching and ion implant. The photolithography process can be broken down into eight basics steps as shown in Figure 11 [25].

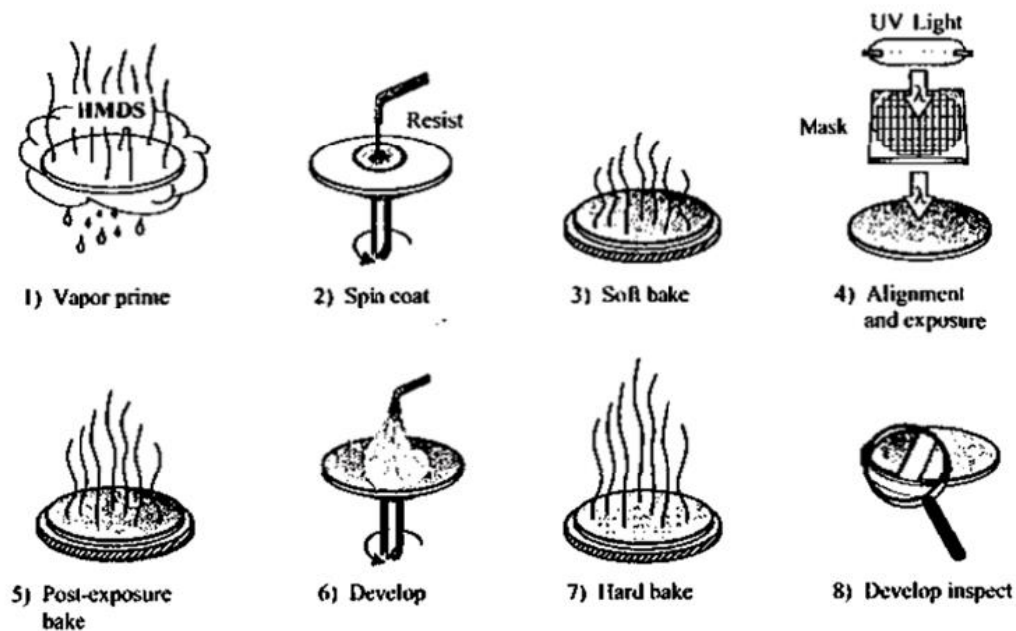


Figure 11. Illustration of the 8 basic process steps used in standard photolithography [25].

2.2.2 Metal deposition

There are several ways to deposit metal on to the substrate surface. The four most common ways are evaporation, sputtering, chemical vapor deposition and electroplating. All these processes are referred to as metallization and are used to form interconnecting metal lines between the dielectric layers in the integrated circuits. There are many requirements that need to be met for metals used for this purpose. They need good conductivity, good adhesion to the substrate, and uniform deposition at low temperatures, easy patterning and planarization, good reliability, good corrosion resistance and sufficient mechanical strength [25].

2.3.3 PDMS

PDMS or poly (dimethylsiloxane) is a common polymer material used for microfluidic devices. It has several favorable properties that include low cost, forming an irreversible and leakage free bond to glass, gas permeable, rapid prototyping, optically transparent and good mechanical strength [26]. The main reason for PDMS being used for micro-fabrication is the combination of easy rapid prototyping and low cost. This combination is very advantageous especially for research purposes as compared to the previously used alternatives such employing glass and silicone. Another advantage is that the molding process for PDMS does not require a cleanroom for dimensions relevant for the microfluidic scale and can be done at low temperature without the use of aggressive chemicals [26,27].

3 Experimental

3.1 Production of MFFC

The experimental methods used for the production of the MFFCs are based on work previously done by Christine Møinichen [28] and later improved by Thomas Holm and the author [29]. The production of electrodes, PDMS-masters, PDMS-channels and some of the assembly were performed in NTNUs ISO certified cleanroom, Nano Lab. A detailed step-by-step production procedure is found in Appendix A.

Table 1 and 2 lists respectively the instruments and chemical used for the production of MFFCs that would exceed what would be considered normal laboratory equipment.

Table 1. Instruments used for the manufacturing of MFFC.

Instrument type	Modell	Manufacturer
Plasma cleaner	Femto	Diener Electronics
Mask aligner	MA6	Karl Süss
E-beam evaporator	Vacuum Classic 500	Pfeiffer
Profilometer	Detak 150	Veeco

Table 2. Chemical used for the manufacturing of MFFC.

Chemical type	Brand name	Manufacturer
Photoresist	ma-405	Micro resist technology GmbH
Developer	ma-331/s	Micro resist technology GmbH
Photoresist remover	Mr-REM-660	Micro resist technology GmbH
Photoresist	SU-8 2100	MicroChem Corp.

Developer	Mr-DEV-600	Micro resist technology GmbH
Silicon elastomer base	Sylgard® 184 Silicone elastomer kit BASE	Lindberg og Lund AS
Silicon elastomer curing agent	Curing agent	Dow Corning S.A
Silicon wafer	Polished Silicone wafers 2", $t = 1 \text{ mm}$	Siltronix

Production of electrodes

The MFFCs were produced using established in-house photolithography methods at NTNU Nanolab. All work with production of electrodes was performed in ISO 5+6 certified cleanroom. All work with undeveloped photoresist was done in an area with UV-filtered light.

Glass slides were cut (2.5 x 3.5 cm) and then cleaned in an ultrasonic bath using, first acetone (5 min., med. intensity) and then isopropanol (5 min, med. intensity). After each cleaning step the slides were dried using N₂ gas. The slides were then cleaned using a plasma-cleaner (10 min., 50% O₂, 50 W) and baked using a heating oven (10 min., 200 °C)

Photoresist (ma-405) was applied to the clean slides using spin coating (30 sec., 1000 rpm, 250 rpm s⁻¹). The slides were thereafter baked using a hotplate (60 sec., 100 °C).

The glass slides were placed in the mask aligner and exposed to UV-light (400 mJ cm⁻²), using a custom made mask and a SOLARONIX UV-filter to reduce reflections. After exposure, the glass slides were developed (ma-D331/s) using visual inspection for endpoint detection (approx. 150 sec.). The slides were then immediately rinsed in water, dried using N₂ and cleaned using a plasma-cleaner (10 min., 50% O₂, 50 W).

The glass slides were mounted and inserted into the e-beam evaporator and a layer of titanium (10 nm) and platinum (190 nm) was deposited. Excess metal was removed

using a photoresist remover (mr-REM-660). The glass slide with the deposited electrodes was inspected for defects using a light microscope.

Production of PDMS-master

The silicon wafer was cleaned in the same manner as the previously mentioned glass slides every step up to application of photoresist. Photoresist (SU8-2100) was applied using a spin coater in a two-step program (Step 1: 10 s, 500 rpm., 100 rpm.s⁻¹. Step 2: 30 sec., 3000 rpm., 300 rpm.s⁻¹). The wafer was then baked using a hot plate in a two-step process (Step 1: 65 °C, 5min. Step 2: 95 °C, 25 min.).

The wafer was placed in the mask aligner and exposed to UV-light (250 mJ cm⁻²), using a custom made mask and then baked using a hotplate (65 °C, 11 min.). After baking the glass slides were developed (Mr-DEV-600) using visual inspection for endpoint detection (approx. 12 min.). The wafer was then hard-baked using a hotplate (150 °C, 15 min.).

Production of PDMS-channels

Silicon elastomer base (25 g) was mixed with silicon elastomer curing agent (2 g) and degassed under vacuum (15 min.). The PDMS master was then placed in a plastic dish and covered by the degassed mixture. The plastic dish was then degassed (30 min.) and heat treated using a heating oven (40 min., 80 °C). The cured PDMS was removed from the dish and PDMS-master and cut into appropriate size. Two holes were made for the one for the reservoir ($D = 2$ mm) and one for the plastic tube ($D = 0.5$ mm) in each end of the channel.

Assembly of MFFCs

The surface with the PDMS-channel was activated using plasma cleaner (24 s, 100% O₂, 20 W), and mounted on top of the electrodes. The cell was then heat treated using a heating oven (40 min., 80 °C).

The tube and reservoir was fastened to the cell using silicon glue and electrical wires soldered to the electrode surfaces. Figure 12 shows a picture of a finished cell

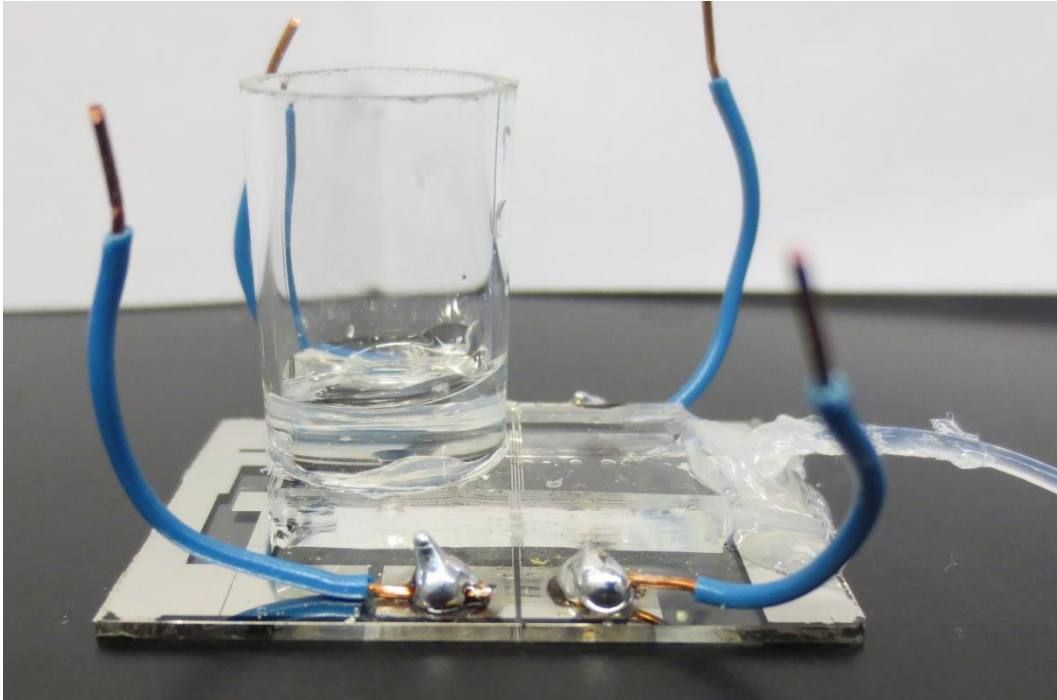


Figure 12. Picture of a fully assembled MFFC.

3.2 Electrochemical experiments.

Table 3 and Table 4 lists respectively the instruments and chemicals used for electrochemical study of MFFCs that exceeds what would be considered normal laboratory equipment

Table 4. Instruments used for electrochemical study of MFFCs.

Instrument type	Model	Manufacturer
Water cleaning system	Mil-Q water system CDOF 01205	Millipore
Syringe pump	PHD 2000	Harvard Apparatus
Potentiostat	Reference 600 Potentiostat/Galvanostat/ZRH	GAMRY instruments

Table 5. Chemicals used for electrochemical study of MFFCs.

Trade name	Purity	Supplier
Hexaammineruthenium(III) chloride	>98%	Sigma-Aldrich
Hexaammineruthenium(II) chloride	>99.9%	Sigma-Aldrich
Potassium sulfate	>99.5%	AnalaR
Potassium iodine	>98.5%	CALEDON
Potassium ferrocyanide	>99.0	Acros organics
Potassium ferricyanide	>99.0	Acros organics
Sulfuric acid	Baseline	Seastar Chemicals Inc.
Potassium nitrate	>99.0	ACP
Potassium chloride	>99.0	ACP

Due to the nature of the experiments several methods have been applied. The method described in this section is the up-to-date standardized method used to collect most data for the MFFCs. Other similar methods used the ferrocyanide/ferricyanide couple as a replacement for the ruthenium (II/III) redox couple.

All solutions were made using deionized water from Mil-Q water systems and purged using argon.

The MFFC was mounted inside the environmental chamber attached to a syringe containing argon-purged deionized water mounted on to the syringe pump as shown on Figure 13.

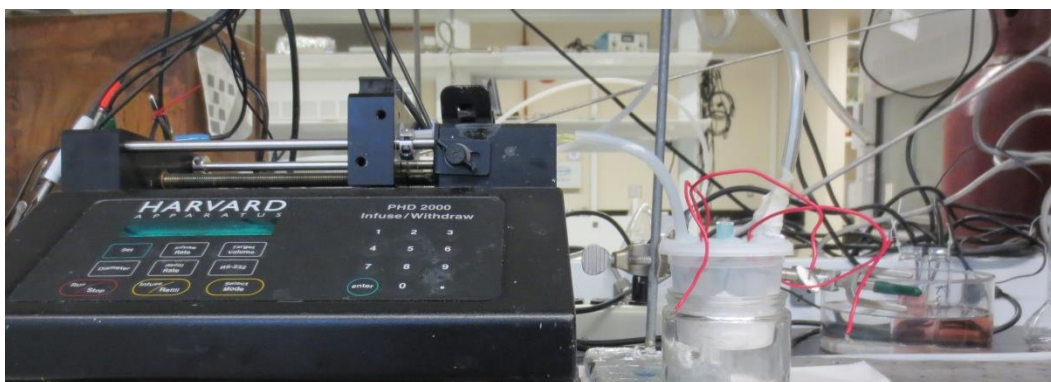


Figure 13. Experimental setup for electrochemical characterization of MFFCs, including a syringe pump and an environmental chamber.

The cell was then purged of oxygen (approx. 2h) using a steady state flow of argon-purged deionized water ($10 \mu\text{l min}^{-1}$.) and an argon flow to the environmental chamber. A base-line was then established using H_2SO_4 (0.2 M) and an external reversible hydrogen reference electrode.

Electrodes 1-3 was then coated with iodine, using a solution of KI (4 mM) and H_2SO_4 (0.5 M) at a constant flow ($10\mu\text{l min}^{-1}$.). The potential at the electrodes were held at a constant potential (6 min., 0.4 V vs. E.ref.) using an external reversible hydrogen reference electrode. The external reference electrode was made using wire platinum

inside a sealed glass tube. Hydrogen was produced and kept in equilibrium with sulfuric acid of the same concentration of that in the MFFC.

The quality of iodine layer was evaluated by comparing new cyclic voltammetry data from capacitance region (0.3 – 0.7 V vs. E.ref.) in H₂SO₄ to the previously established base-line.

The electrolyte was then changed to the ruthenium complex using an internal reference electrode and several of electrochemical experiments were performed, including cyclic voltammetry and electrochemical impedance spectroscopy. After experiments the iodine layer was re-evaluated in the same manner.

4. Results and Discussion

4.1 Redesign of PDMS masters

The method for producing PDMS masters was redesigned using circular silicone carrier wafers ($D = 2.54$ cm) instead of small glass slides (2×2 cm). The change in methodology was prompted due to the poor durability of the previous design. Repeated use and heat treatments caused the epoxy-based negative photoresist SU-8 to loosen from the glass slide.

According to the manufacture's details [30], the SU-8 adhesion to silicon is greater than glass. In addition, the circular shape of the silicon wafer prevents buildup on the corners, giving the channel a more uniform height. Figure 14 shows an example of two height profiles: one for the square glass slides and one for the circular silicon wafers. The figure clearly shows the effects that the edges and corners have on the channel profile, and the advantage of using a circular oversized master.

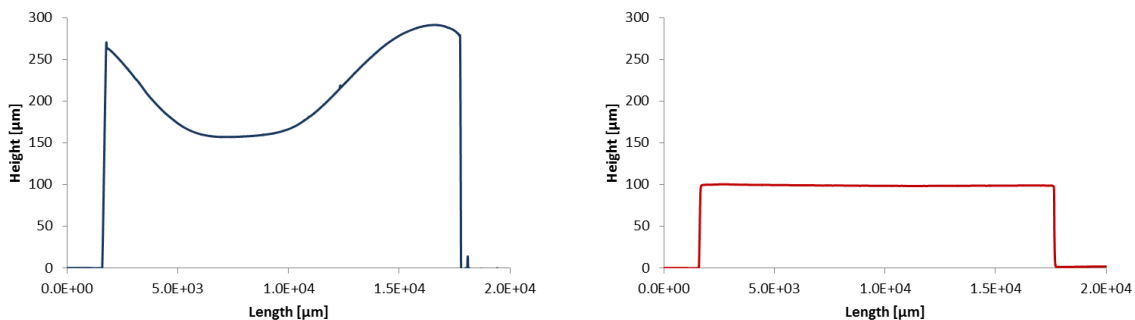


Figure 14. Height profiles of PDMS masters using small glass slide (blue) and circular silicon wafer (red).

An additional advantage of using silicon wafers compared to glass slides is the contrast during the alignment step of the PDMS master manufacturing. Due to the viscous nature of the SU-8, bubbles causing deformation of the channel have previously been a problem. The increase in contrast allows bubbles to be observed during alignment and thereby be avoided.

Originally regular silicon wafers were used, but due to the lack of structural integrity they were often damaged during the removal of PDMS. A carrier wafer is a much thicker wafer ($t = 1 \text{ mm}$) giving the master the necessary structural strength for repeated use.

The adhesion between silicone and SU-8 has proved to be a substantial improvement over the SU-8 to glass bond, allowing repeated production of PDMS channels without damaging the master.

The new method for the production PDMS masters gives better durability and produces PDMS channels of a higher quality. The increase of durability decreases the total time for the production of the MFFCs significantly as the production of PDMS masters was a significant part of the original procedure.

4.2 Gold-platinum electrode characteristics

To minimize electrode resistance, electrodes consisting of an adhesion layer of titanium (10 nm), a conducting layer of gold (140 nm) and a surface layer of platinum (50 nm) were constructed. The resistivity of platinum is about five times as high as gold. Using electrodes combining a conductive core of gold electrodes allows the resistance to be lowered to about 30% of that of pure platinum electrodes

During initial testing of MFFCs in the previous project work of the author [29], a platinum layer of 10 nm was used in combination with gold. However some of the cells showed current peaks associated with the reduction and oxidation of gold oxide. The peaks were thought to be caused by either damage to the platinum surface during construction of the MFFCs or dissolution of platinum during the electrochemical experiments. As a result the thickness of platinum was therefore increased to 50 nm when the experiments continued during the winter of 2014 and this thickness was adopted as a standard.

While working on establishing a correct voltammogram of the Pt surface in sulfuric acid, the electrodes clearly showed voltammetric features associated with formation and reduction of gold oxide. The current associated with these peaks continued to grow with increasing cycle numbers. This indicates only partial coverage of the gold substrate with the thin Pt layer, which degraded even more with time. This behavior was observed for several MFFCs. Figure 15 shows two cyclic voltammograms for the same MFFC in the same electrolyte with a time interval of approximately 30 min. The cell was in constant use in the relevant time interval and used an external reversible hydrogen electrode.

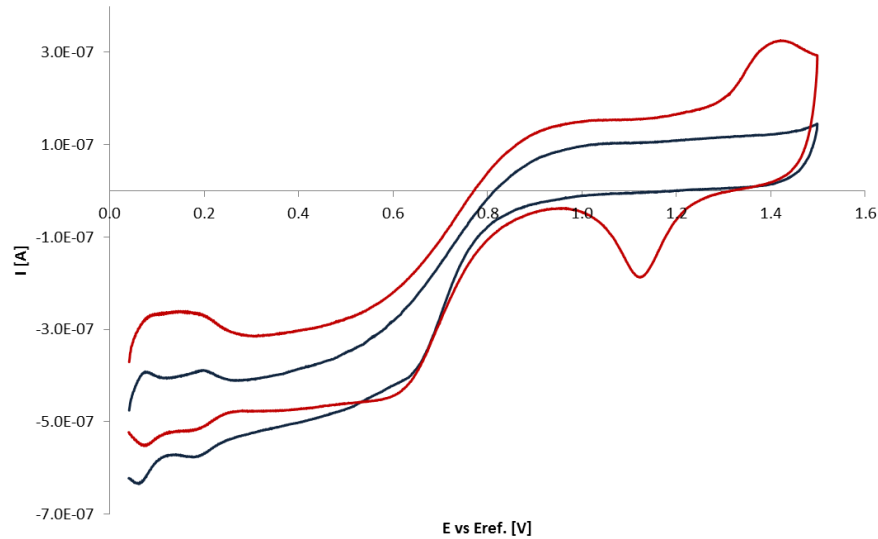


Figure 15. Cyclic voltammetry data for MFFC with platinum-gold electrodes in sulfuric acid at two different time intervals using an external reversible hydrogen electrode. Showing the initial results ($t = 1$ min. blue) and results after several electrochemical experiments ($t = 30$ min. red).

To identify the problem, the PDMS was removed from the channel and the area of the electrodes exposed to the channel was photographed using a light microscope. Figure 16 shows the picture taken of the electrodes taken using a light microscope. The MFFC was only exposed to sulfuric acid. Electrode 2 was used as working electrode, and electrode 4 was used as counter electrode. The experimental setup included an external reversible reference hydrogen electrode.

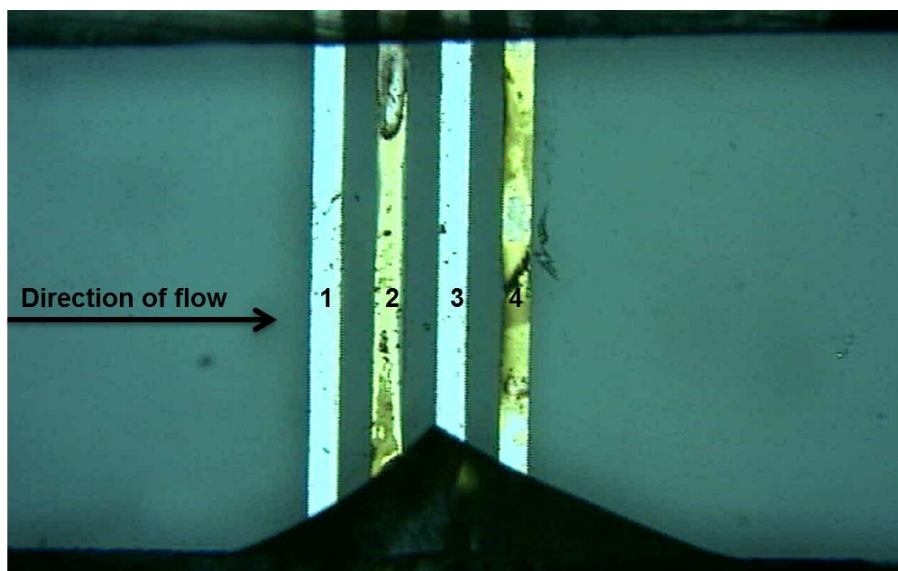


Figure 16. Picture taken using a light microscope of the platinum-gold electrodes after exposure to sulfuric acid. Electrodes 2 and 4 were subject to electrochemical activity and show degradation of the platinum surface layer exposing the layer of gold underneath.

The picture clearly shows the degradation of the surface layer of platinum on the electrodes that had been exposed to electrochemical activity. For electrode 4 in particular the damage seems to be more severe on the edge exposed to the direction of the flow. The electrodes that were not exposed to electrochemical activity seem unaffected.

One possible mechanism for the degradation of the surface layer of platinum is that the lift-off technique used to produce the electrodes leaves an exposed gold surface on the edge of the electrodes as illustrated by Figure 17. When the exposed gold surface oxidizes the expansion of the oxide may cause the platinum to peel off on the edge of the electrode. Another possible mechanism could be that gold is dissolving underneath the platinum layer. This will expose a larger area of gold, and make it more likely that thin platinum will be separated from the rest of the electrode. Both these processes will be helped by the flow and progress from the edge to the center of the electrode.

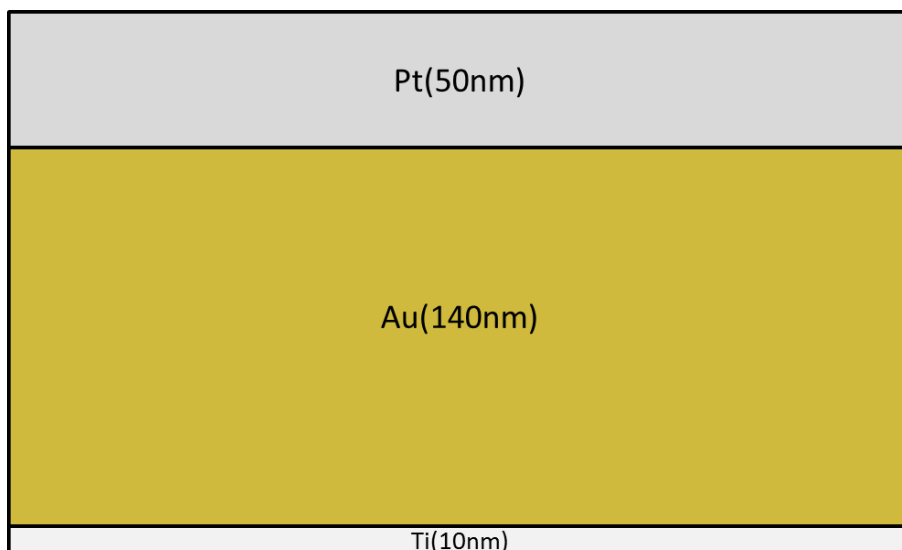


Figure 17. Schematic build-up of the platinum-gold electrodes in the early stages of this work.

Two possible mechanisms for removal of platinum were: damage to the platinum surface during construction or dissolution of platinum during electrochemical experiments. Removal of platinum caused by damage during construction of the MFFCs, seem unlikely due to the significant difference of the surface of the two electrodes not exposed to electrochemical treatment compared to the electrodes exposed to treatment.

Extensive testing on MFFCs with electrodes consisting of a 10 nm titanium adhesion layer and 190 nm platinum surface layer, have showed excellent durability and a near constant surface area over several days of experiments. These observations make it very unlikely that the rapid degradation of the platinum layer of the initial electrodes was caused by dissolution of platinum. An alternative mechanism could be deterioration of the adhesion gold and platinum with the degradation solely due to mechanical removal, due to fluid flow. However, this seems unlikely due to the large difference between the electrodes depending on the exposure to electrochemical treatments.

4.3 Oxygen elimination and proper voltammetric baseline response with a custom-made environmental chamber

Diluted, high purity sulfuric acid is an inexpensive readily available electrolyte with well-defined properties and well-studied interaction with platinum electrodes. It was therefore chosen to establish a proper voltammetric “baseline” for the MFFC electrodes.

The Pt cyclic voltammograms in sulfuric acid are very sensitive to oxygen reduction in the lower potential region. The presence of oxygen will give a relatively large contribution to the current at lower potentials directly depending on the oxygen concentration in the electrolyte. In order to establish a satisfactory baseline condition, the removal of oxygen is essential. Oxygen was removed from the electrolyte by purging electrolyte with argon before entering the MFFC. This approach is commonly used in large vessel experiments. Figure 18 shows a cyclic voltammogram of a Pt electrode in a MFFC using an argon purged electrolyte. The negative shift in the cyclic voltammogram clearly shows a rather large effect of dissolved oxygen. Thus standard purging was insufficient to remove all the oxygen from the system and obtain the desired baseline conditions.

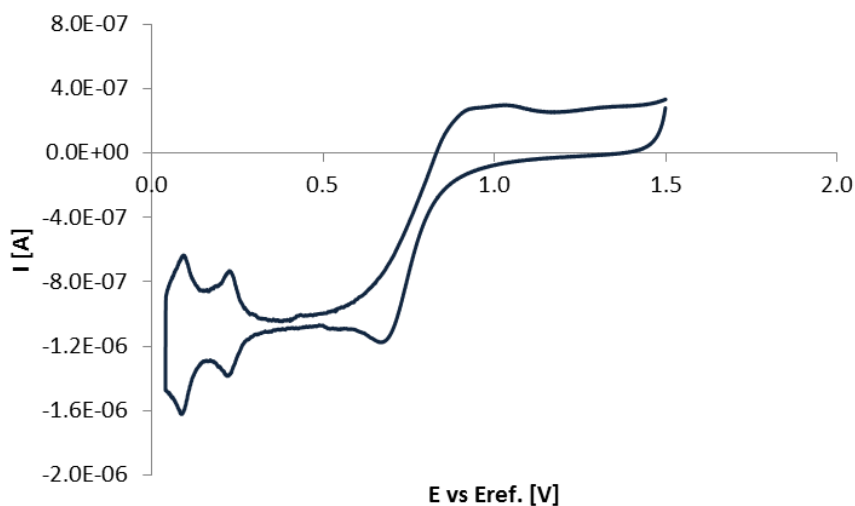


Figure 18. Cyclic voltammogram of a Pt electrode in a MFFC at 200 mV s^{-1} using argon-purged 0.2 M sulfuric acid and an external reversible hydrogen reference electrode. Data is collected before purging of the environmental chamber.

PDMS is permeable to oxygen and has been used as an oxygen membrane. In order to prevent the free access of oxygen to the surface of the PDMS and thereby prevent the transport of fresh oxygen through the membrane the MFFC was fitted inside a small custom-made environmental chamber. The chamber was continuously purged with argon creating an oxygen-free environment. The chamber included an Ar-purged outer tube surrounding the Teflon tube for fluid delivery from the syringe to the cell to prevent possible transport of oxygen through the Teflon tubing. To minimize the necessary interaction inside the chamber after mounting the cell, the box included internal wires that could be attached to the cell and accessed and switched from the outside without opening the chamber and exposing the MFFC to the oxygen in the ambient environment. An easy access to the reservoir was also created in order to ease the emptying of the reservoir and mounting of external reference electrodes. Figure 19 shows a picture of the chamber with a mounted MFFC inside.

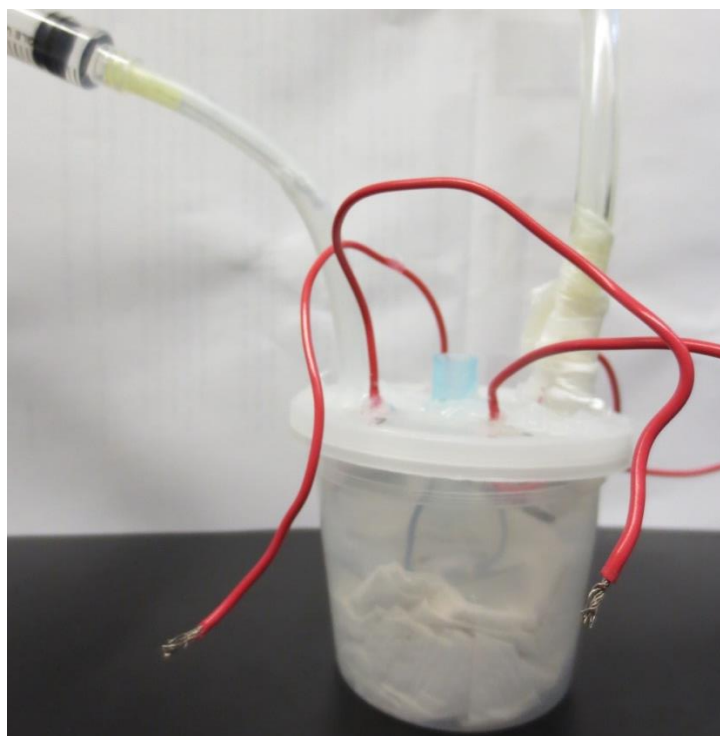


Figure 19. Picture of the custom-made environmental chamber creating an oxygen-free environment for the MFFCs.

After placing the cell with an oxygen-free electrolyte in the oxygen-free environment initial experiments in sulfuric acid still showed substantial amounts of oxygen present. However, after using continuous flow of the electrolyte, oxygen levels in the system were slowly depleted and a satisfactory voltammetric baseline was achieved.

Figure 20 shows the magnitude of contribution of the oxygen reduction current at different time intervals in oxygen-free sulfuric acid. The electrolyte had a constant flow ($10 \mu\text{l min}^{-1}$) and was placed in the oxygen-free box at $t = 0$ min. The figure clearly shows that there is no significant difference between the starting conditions and the 1 min. interval. Due to the size of the box, removal of oxygen should only take a few seconds, however the oxygen reduction current is almost unaffected. The time required to remove all the oxygen from the system was about 2 h. The continuous flow of electrolyte verifies that the oxygen reduction current is not due to remaining oxygen in the electrolyte.

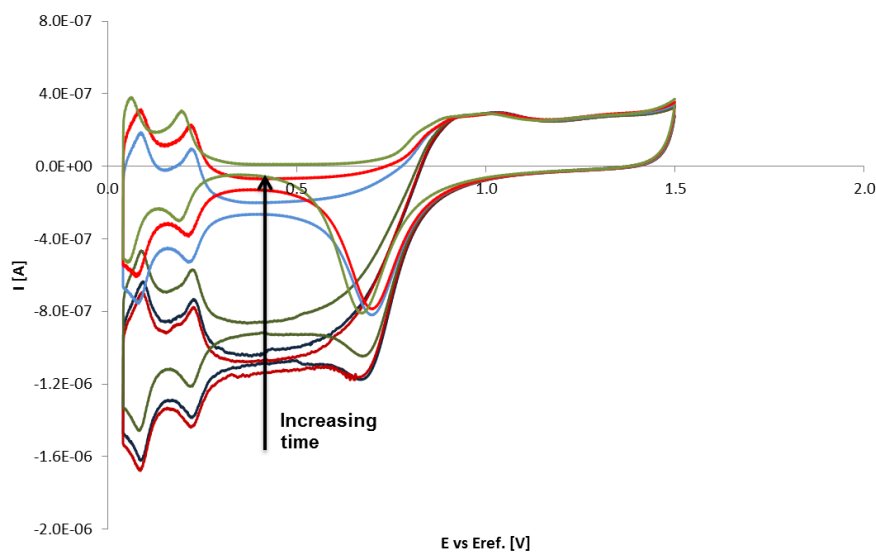


Figure 20. Cyclic voltammograms for five different time intervals (0 min. dark blue, 1 min. dark red, 5 min. dark green, 15 min. blue, 60 min red and 90 min. green) of purging of environmental chamber surrounding MFFC at 200 mV s^{-1} using argon-purged 0.2 M sulfuric acid in MFFC using an external reversible hydrogen reference electrode.

The most plausible explanation for the results is that PDMS is saturated with oxygen, giving rise to a slow supply of oxygen to the oxygen-free electrolyte. Oxygen will be

leaking out into the electrolyte until the PDMS is depleted. The dimension of the channel gives a high surface area to volume ratio that increases the diffusive flow of oxygen to the electrolyte. To verify this hypothesis a subsequent experiment was set up. The cell was first purged with argon and there was continuous flow of oxygen-free deionized water. After 2h the electrolyte was changed to oxygen-free sulfuric acid. The voltammogram showed no oxygen reduction, which supports this hypothesis. This method for removing oxygen has been incorporated as part of the standard procedure when running experiments using MFFCs.

Figure 21 shows a baseline cyclic voltammogram in sulfuric acid achieved using this procedure. A small amount of oxygen remains. The diffusion-limited oxygen current can be estimated by taking the mean of the currents on the positive-going and negative-going sweep at 0.4 V, and is seen to be slightly negative on the voltammogram shown. The difficulty of removing oxygen may explain why Pt electrodes are used less commonly than gold for electroanalytical applications, and literature results for experiments at Pt microelectrodes often show trace oxygen [31].

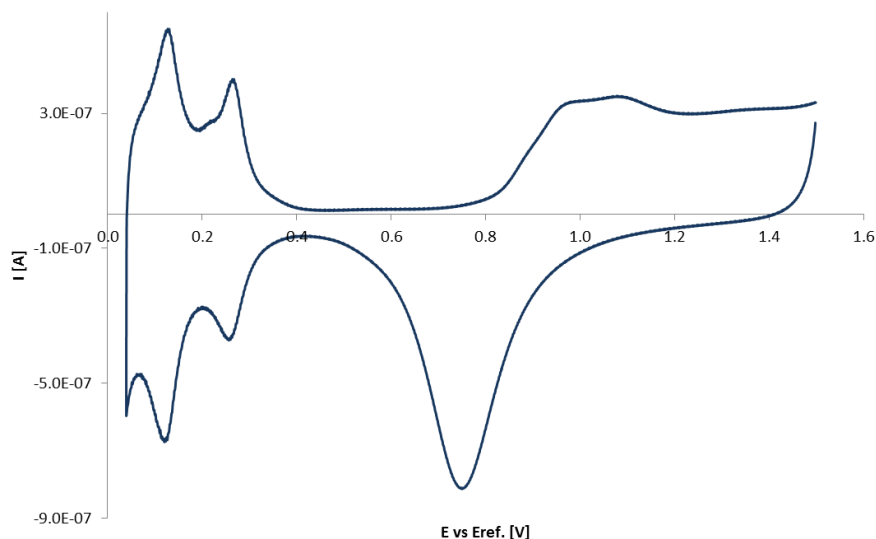


Figure 21. Example of baseline established prior to experiments after removal of oxygen in MFFCs using 0.2 M sulfuric acid and an external reversible hydrogen electrode.

4.4 The ferricyanide/ferrocyanide redox couple

Initial experiments using the ferricyanide/ferrocyanide redox couple show peak separations inconsistent with expected reversible behavior. The electrodes also showed a decrease in estimated surface area. The most plausible explanation for both these effects is the buildup of Prussian blue of the electrode surface.

The Prussian blue layer on the surface inhibits surface activity and is hard to remove using techniques that are compatible with MFFC. Therefore the best option is to prevent the buildup.

In the literature it has been suggested that the presence of a monolayer of iodine on the surface of Pt electrodes can prevent build-up of surface species such as Prussian blue. Preventing this build-up should yield near ideal reversible behavior of the ferricyanide/ferrocyanide redox couple.

After establishing a method for depositing an iodine layer, a series of experiments was performed using a conventional electrochemical glass cell. The method for depositing the iodine layer will be discussed later. A series of experiments compared two platinum electrodes in the same electrolyte. Where one had an iodine layer deposited and the other was a clean platinum electrode. Figure 22 shows a cyclic voltammogram for each electrode at 200 mV s^{-1} for the ferricyanide/ferrocyanide redox couple. It is worth noting that the surface areas of the two electrodes were different causing the observed difference in measured current. However the peak separations of the two different electrodes are similar and larger than expected assuming ideal reversible behavior.

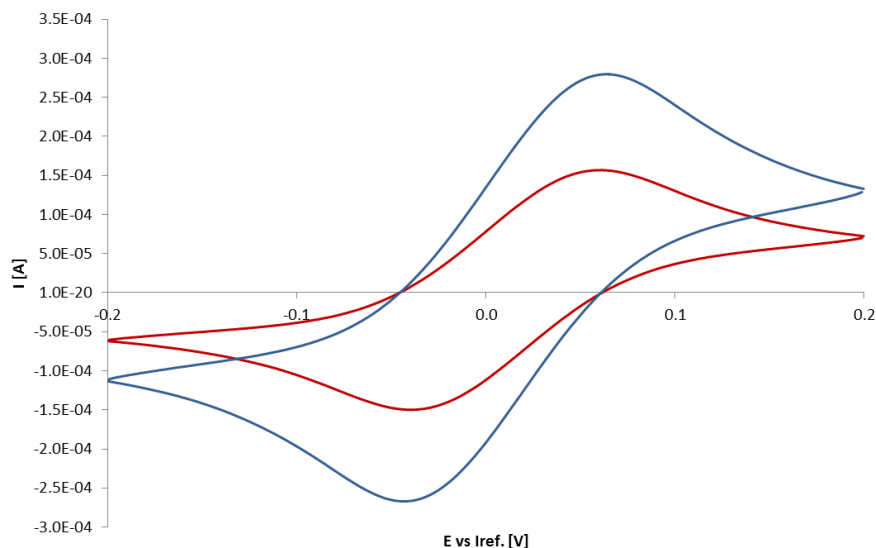


Figure 22. Cyclic voltammograms for the ferricyanide/ferrocyanide couple using one clean platinum electrode (red) and one iodine-coated platinum electrode (blue) at 200 mVs^{-1} using an internal reference electrode.

It is not clear if the non-ideal behavior of the iodine-coated electrode is caused by the electrode being exposed to ferrocyanide prior to the experiment, the iodine layer being damaged, or the iodine layer being unable to prevent the build-up of Prussian blue.

The use of ferrocyanide was rejected from further studies due to the inability to obtain reversible behavior and the buildup of Prussian blue inhibiting electron transfer.

4.5 The ruthenium redox couple.

Due to the observed irreversible behavior of the ferricyanide/ferrocyanide couple. An alternative redox couple was investigated. The ruthenium hexaammine (II/III) redox couple is a commonly used reversible (fast) redox couple that was previously being used in MFFCs by Kjeang et al. who obtained near reversible behavior.

Unfortunately the ruthenium redox couple is sensitive to room temperatures and air making it rather instable under ambient laboratory conditions. Visible changes to the color of the solution were observed after a few hours of operation, and certain precautions were therefor introduced. Keeping the solution cooled (on ice) decelerated the decomposition process.

Initial experiments showed a small degree of irreversibility and a small decrease in current over time. Reevaluating the electrode by comparing to the baseline behavior showed a general minor passivation effect and some additional activity in the oxidation region. A possible explanation for this is ruthenium oxide depositing on the surface, causing a minor passivation effect. Extensive cycling of the electrode in sulfuric acid returned the electrode to its previous Pt baseline behavior.

The effect of the iodine monolayer on the platinum electrode was investigated on the ruthenium redox couple. Figure 23 shows the cyclic voltammograms for the same electrode coated and uncoated with iodine in the ruthenium redox solution. Both the coated and uncoated electrodes show near ideal reversible behavior. However the electrode coated with iodine has slightly lower peak separation and the side reaction at lower potentials is less pronounced. In addition, when comparing the electrodes to the baseline behavior in sulfuric acid, the iodine-coated electrode showed little to no passivation and no additional oxidation activity was observed. It was therefore decided to incorporate the use of iodine in conjunction with the ruthenium redox couple as part of the standard procedure.

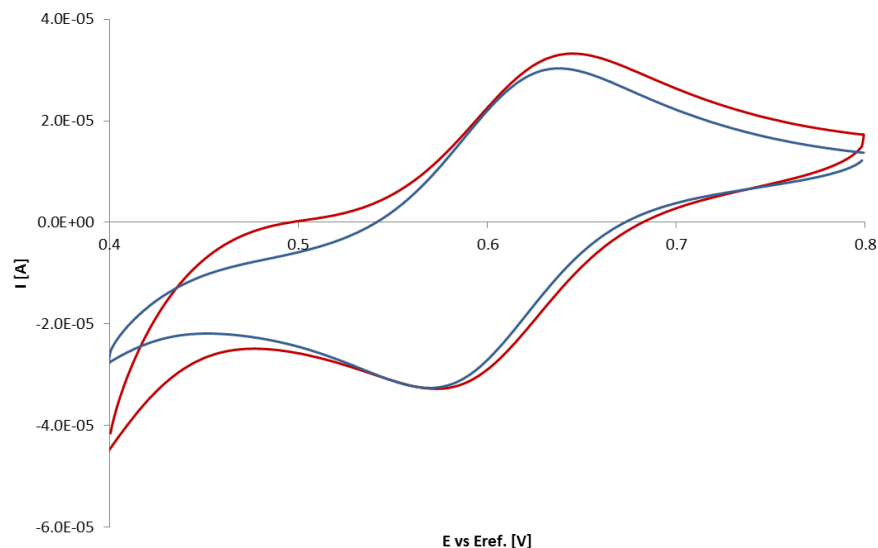


Figure 23. Cyclic voltammogram for the ruthenium couple using one iodine-coated platinum electrode (blue) and one uncoated platinum electrode (red) at 200 mV s^{-1} using an external reversible reference electrode.

The concentration of the ruthenium-complex was 1 mM of each complex in a supporting electrolyte of 0.5 M K_2SO_4 . At these concentrations it proved difficult to establish a stable open circuit potential. The instability of the open circuit potential was especially evident when using an internal reference electrode and the instability prevented any relevant experimental data from being extracted. It was possible to obtain some data using an external reference, however these data were not of satisfactory quality due to the signal to noise ratio. It is reasonable to assume that the low concentration of the redox couple caused it not to be the sole dominating reaction on the electrode surface and thereby limiting its ability to control the potential at the reference electrode. Other competing reactions such as oxidation of the platinum surface or a mixture of other unknown reaction caused either by the iodine layer or the ammine ligands could take place at the surface and shift the open-circuit potential. This problem was avoided by increasing the concentration of the redox to 5 mM for each species. This increase allowed the redox couple reaction to be the dominating reaction at the surface and gave a stable potential. All further experiments using the ruthenium redox couple were done at 5 mM concentration of each species.

4.6 Deposition and stability of the iodine layer.

Several methods for depositing iodine on Pt are proposed in the literature. These include both methods where the potential is controlled and simpler methods where the electrode is exposed to the iodine solution at the open-circuit potential. However controlling the quality of the surface layer or the amount of deposited iodine is difficult. The methods described in literature for determining the amount of deposited iodine requires the removal of the iodine layer, making it impossible to characterize the layer prior to experiments.

Initial tests for determining the optimal method of deposition were done in a standard electrochemical glass cell. Three different methods were evaluated at different time intervals. These three methods were: immersion in KI, immersion in a mixture of KI and I₂ followed by a shorter immersion in KI, and constant potential deposition in a mixture of KI and sulfuric acid.

The quality of the deposited iodine layer was determined by three methods: i) the reduction of capacitance current, ii) stripping the iodine using chronoamperometry and estimating the total charge, and iii) the reduction of the hydrogen underpotential adsorption peaks in sulfuric acid. Figure 24 to 26 shows an example of each of the three methods, compared to the same electrode uncoated in the same electrolyte for reference. All methods clearly show the influence of iodine. Figure 24 shows a clear reduction of the hydrogen absorption and desorption peaks for the electrode coated in iodine. Figure 25 shows currents between 1.2-1.5 V vs. external reversible hydrogen electrode, associated with stripping of the iodine layer. Figure 26 shows a substantial reduction of the capacitance current for electrode coated in iodine.

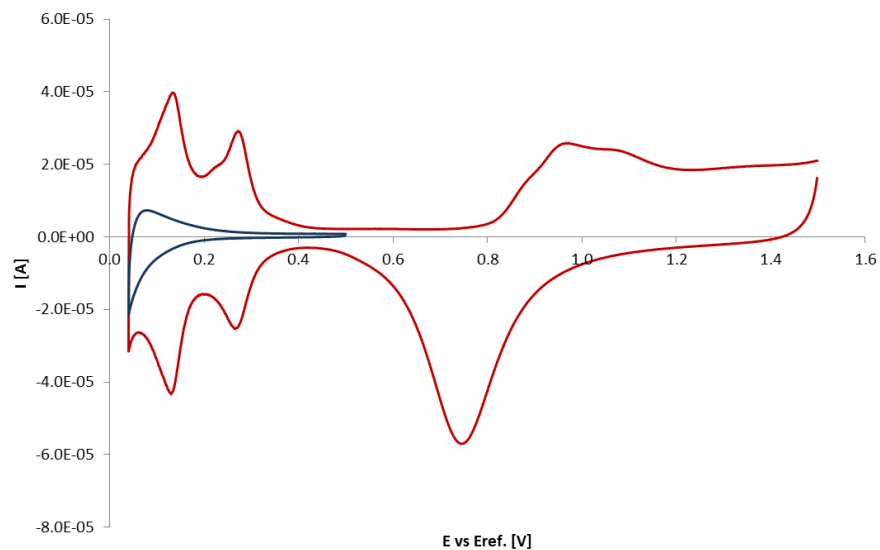


Figure 24. Cyclic voltammogram for a platinum electrode in sulfuric acid in a glass cell, showing an iodine-coated electrode (blue) and an uncoated electrode (red) using an external reversible hydrogen electrode at 200 mVs^{-1} .

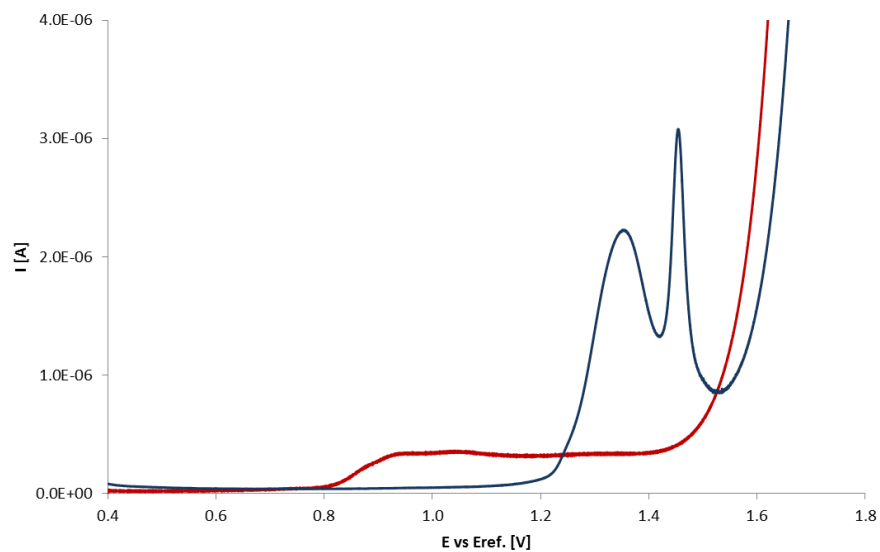


Figure 25. Linear-sweep voltammogram for a platinum wire electrode in sulfuric acid in a glass cell, showing an iodine-coated electrode (blue) and an uncoated electrode (red) using an external reversible hydrogen electrode at 2 mV s^{-1} .

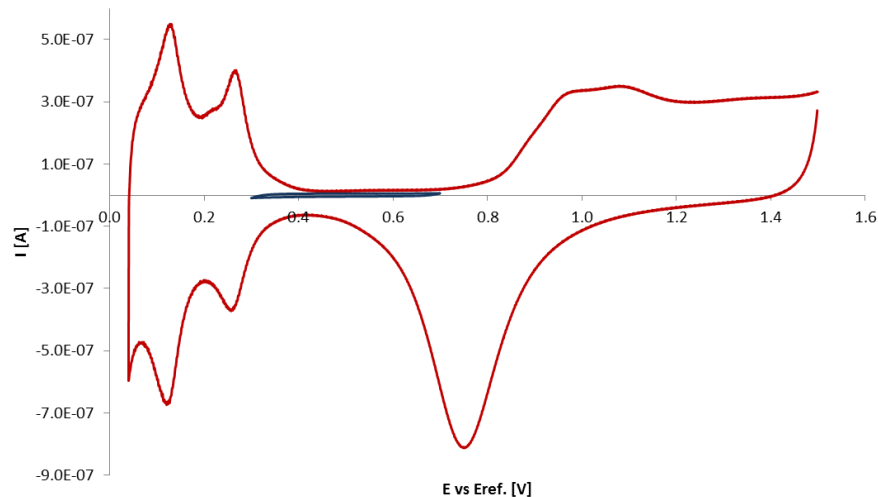


Figure 26. Cyclic voltammogram for platinum wire electrode in sulfuric acid in a MFFC, showing an iodine-coated electrode (red) and an uncoated electrode (blue) using an external reversible hydrogen electrode at 200 mV s^{-1} .

The method of using the capacitance current to characterize the iodine layer was incorporated as part of the standard experimental setup. It was the least destructive method for the iodine layer, and could be used prior to the electrochemical experiments. However, both the methods evaluating the capacitance current and the hydrogen adsorption peaks are not ideal, as they are hard to differentiate from normal passivation of the electrode surface due to impurity adsorption. This makes it challenging to make a good evaluation of the quality of the surface layer using these methods.

The method of electrochemical deposition rather than deposition at the open-circuit potential was chosen on the basis of evaluating the results from the three different methods. Both the quality of the iodine layer and the time necessary to achieve the desired result contributed to the choice of method. This chosen method is described in the experimental section.

An iodine-coated electrode operating at its open-circuit potential was used to determine the stability of the iodine layer during electrochemical experiments. This electrode was used as a reference to decide whether the degradation of the iodine layer was caused

by the surface processes associated with cyclic voltammetry and impedance spectroscopy or due to the exposure to the electrolyte alone. The electrode left at open-circuit showed little to no increase in capacitance current. However the electrode used as the working electrode for the electrochemical experiments showed a significant increase in capacitance current. These results clearly indicate that the potential of the electrode is a determining factor for the stability of the iodine layer.

The stable potential window for the iodine layer was estimated by cyclic voltammetry. Several potential windows in both sulfuric acid and supporting electrolyte (potassium sulfate) were investigated. The results indicate that the iodine is oxidatively removed at potentials not much higher than the reversible potential of the ruthenium complex. By restricting the potential limits within the stable potential window of the iodine layer it was possible to maintain a low capacitance current and the absence of hydrogen peaks.

However, some experiments with the same potential limit, and timeframe yielded different results for the degradation of the iodine layer. One possible explanation for this is loss of potential control during the experimental procedure. This can occur either between experiments or during experiments. A shift in the open-circuit using an internal reference electrode of a few hundred millivolts has been observed when measuring the open-circuit potential between experiments. Such a shift of rest potential can jeopardize the integrity of the iodine layer. The reason for such a shift in potential is unknown. Possible explanations may be the presence of unknown surface reactions, local changes in concentrations at the electrode surface, or effects caused by the decomposition of the electrolyte.

Later experiments showed some increase in capacitance current after the electrochemical experiments indicating that the iodine layer had been partly removed or damaged showed most of the desired effects associated with the layer. This indicates that a fully coated surface is not necessary to achieve the desired effect of the iodine layer.

4.7 Positioning of the reference electrode and resistance measurements in MFFCs

In electrochemical measurements performed in standard electrochemical glass cells, the reference electrode is typically situated between the working and counter electrodes. In general for such experiments, the placement is not of great significance to measurements as long as the conductivities of the electrolyte and electrodes are high. In the case of MFFCs the current pathways are far more restricted making the location of the reference electrode more important.

For the case involving an internal reference electrode, Figure 27 and 28 show the impedance measurements for a MFFC design B, together with the electrode configuration. The reference electrode (R) is marked red, working electrode (W) green and counter electrode (C) yellow. These two electrode setups will later be referred to as electrode setup 4 and 9 respectively.

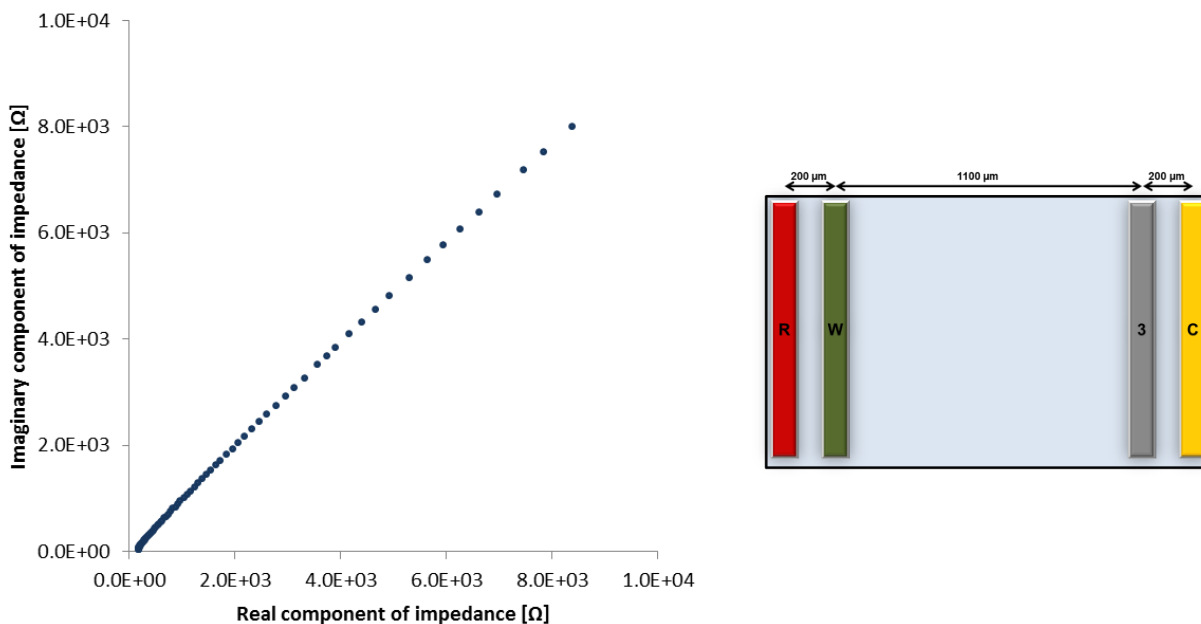


Figure 27. Impedance measurements for ruthenium redox couple using iodine-coated platinum electrodes together with relevant electrode setup.

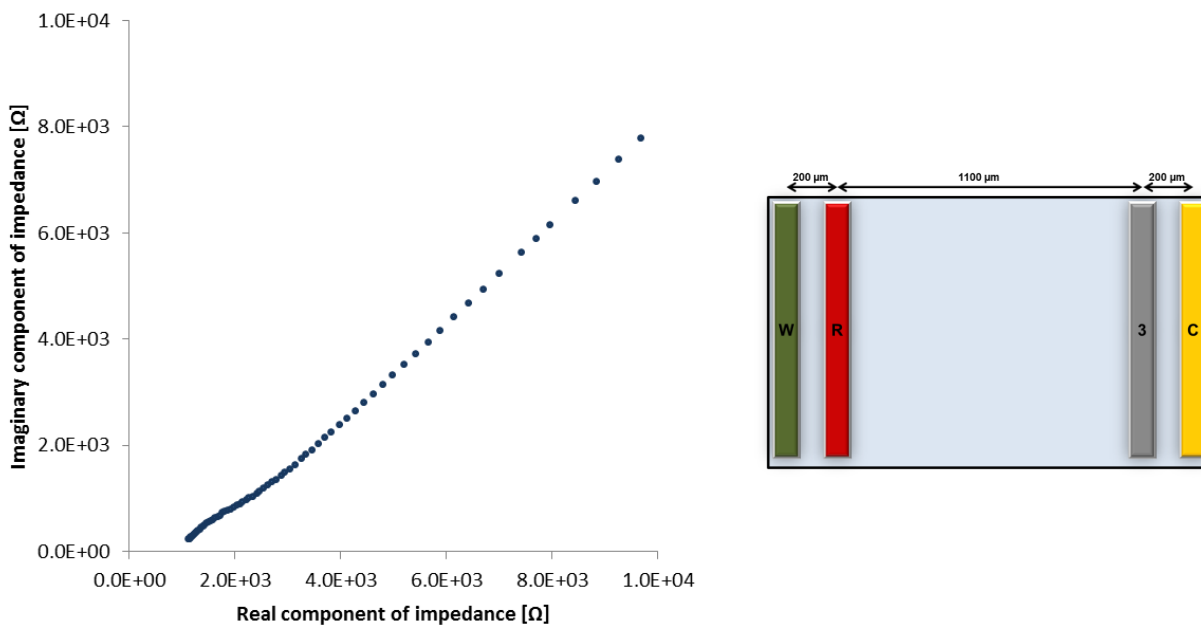


Figure 28. Impedance measurements for ruthenium redox couple using iodine-coated platinum electrodes together with relevant electrode setup.

The placement of the reference electrode determines the potential sensed by the reference electrode, which is determined by the current distribution established between the working and counter electrodes. In the case of MFFCs the small channel forces the current down the channel creating a high current density and a high potential drop over small distances. Due to most of the current being forced straight down the channel, the potential drop on the upstream side of the working electrode is low compared to the potential drop on the downstream side. This allows the reference electrode placed upstream of the working electrode to sense the equipotential line close to the working electrodes surface on the downstream side. Placing the reference electrode between the counter and working electrodes should cause the reference electrode to sense a fraction of the potential drop between the working and counter electrodes consistent with the fraction of the distance between them. It is unknown what interference is caused due to running a high current over the reference electrode. However, at high frequencies some artifacts were sometimes observed. An example of such an artifact is the semi-circle shown in Figure 28. For a highly-reversible redox couple as such ruthenium couple, it is

expected that the reaction is solely mass transport controlled, which should show a straight line at 45° in the Nyquist-plot, as shown in Figure 27.

For the case involving an external reference, similar problems can occur due to the placement of the reference electrode relative to the working and counter electrodes. For experiments involving flow, the working electrode should always be upstream of the counter electrode to ensure that the composition of the electrolyte is not perturbed by reaction products from the counter electrode reaching the working electrode. Likewise the reference electrode should be upstream of the working electrode so that it sees always the same composition. This is however not possible with the current setup-up due to the external reference being placed in the reservoir. Two possible solutions to this problem are to reverse the syringe pump, sucking the solution the opposite way, or to place the reference electrode in the syringe.

The resistance of the system neglecting the electrolyte resistance can be estimated using electrochemical impedance. The equipotential measured by the reference electrode should be equal to potential close the working electrodes surface on the downstream side. This allows the electrolyte resistance to be negligible compare to the contribution from the electric circuits and wiring.

The resistance between the working and reference electrodes was measured using electrochemical by extrapolating the high-frequency spectrum to where it intersects the real axis in the Nyquist-plot. The electrolyte consisted of 5 mM of the ruthenium complex with 0.1 M K_2SO_4 as supporting electrolyte. The setup was varied with several different combinations of electrodes giving different distances between the working and counter electrodes. The reference electrode was always upstream for the working electrode, and the working electrode was placed upstream for the counter electrode. This setup reduces unnecessary interference and should minimize the contribution of electrolyte resistance outside the region with the electrodes. Figure 29 shows schematics of the different cell designs with the relevant distances. Table 5 shows the different setups and the measured resistance based on impedance. The table includes Figures 30 to 35 that

show the electrode setup of each measurement. The working electrode is marked green (W), the counter electrode is marked yellow (C) and the reference electrode is marked red (R). It is worth noting that the two different types of cells can have individual variations in resistance for electrodes and wires. The measurements also allows for the effect of the placement of the reference electrode to be studied.

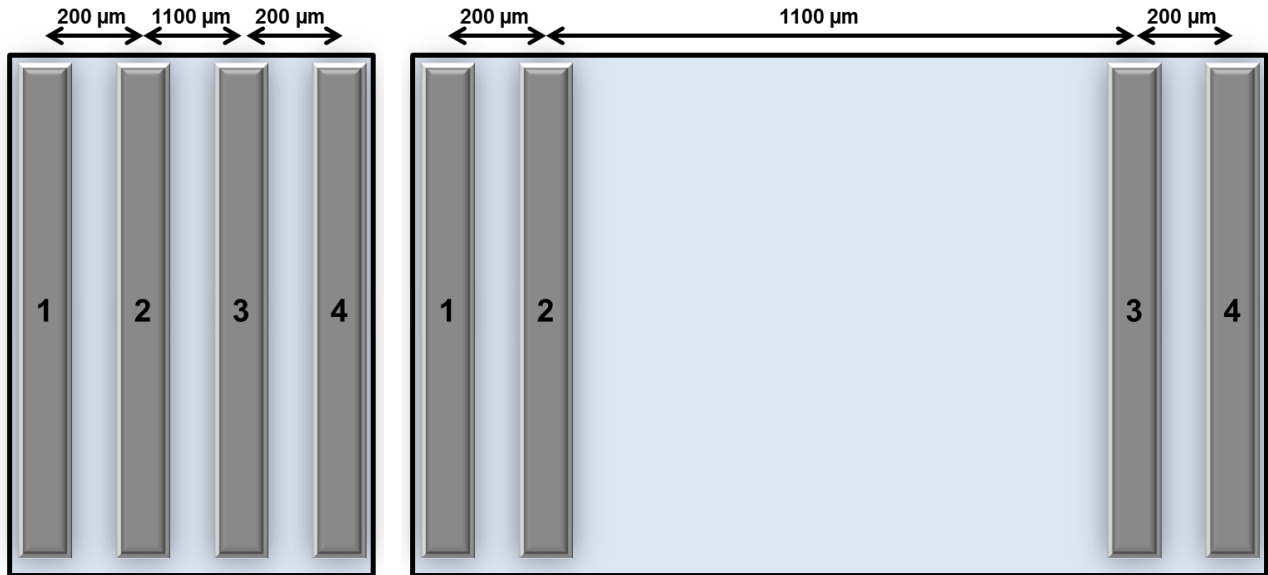
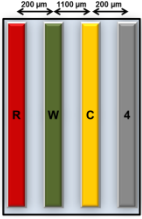
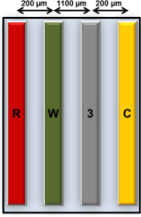
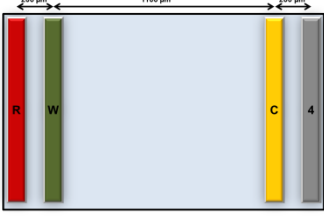
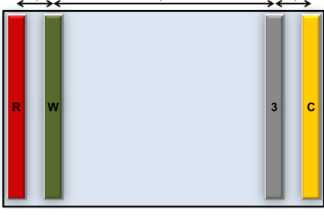
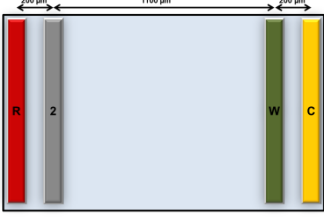
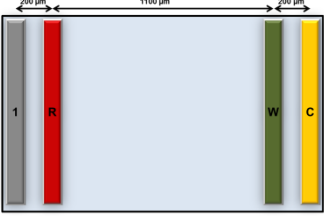


Figure 29. Relevant distances for the two cell designs used in this experiment. Cell design A is on the left, and cell design B is on the right.

Table 5. The table shows measured resistance for two different MFFC designs using several electrode setups.

Electrode setup nr.	Electrode setup	Resistance from impedance [Ω]
1	 <p data-bbox="386 1766 542 1801">Figure 30.*</p>	$1.0 \cdot 10^2$

2	 <p>Figure 31.*</p>	$2.5 \cdot 10^2$
3	 <p>Figure 32.*</p>	$1.3 \cdot 10^2$
4	 <p>Figure 33.*</p>	$1.3 \cdot 10^2$
5	 <p>Figure 34.*</p>	$-6.7 \cdot 10^1$
6	 <p>Figure 35.*</p>	$5.6 \cdot 10^2$
*Electrode setup for MFFC corresponding to impedance measurement.		

The results show that distance between the reference electrode and the working electrode is of important for the impedance measurements. Electrode setup 3 and 4 indicate that stable and accurate measurements can be achieved if the distance

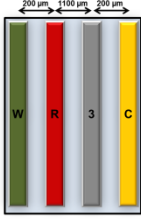

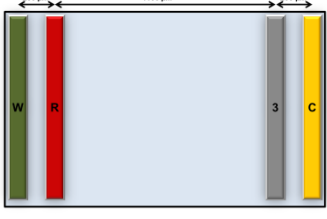
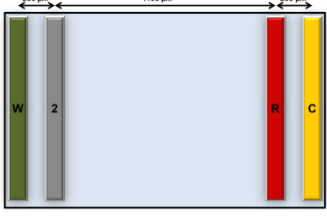
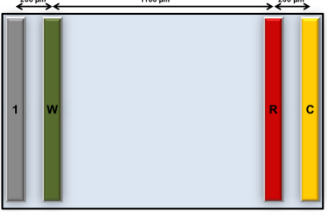
between the working and counter electrode is much greater than the distance between the working and reference electrode. Comparing the results of electrode setup 1 and 2 to 3 and 4, it is evident that the placement of the counter electrode is relevant for impedance measurements if the distance between the counter and working electrode is comparable to the distance between the working and reference electrode.

On the basis of the foregoing reasoning, the shape of the Nyquist-plots and the estimated values it is safe to dismiss the results from electrode setup 5 and 6. The value for resistance estimated from electrode setup 3 and 4 is comparable to what is expected using a wire approximation for the electrodes. It is uncertain if the resistance measured for electrode setup 1 is accurate, due to the factors previously discussed, but it is reasonable to use it as a rough estimate.

Attempts to use an external reference to estimate the systems resistance yielded negative results similar to electrode setup 5. The distance between the working electrode and the reference electrode using an external reference is much greater than the distance in electrode setup 5 and 6. The results indicate that using a cell with a large distance between the working and counter electrode similar to cell design B, could be desirable when performing electrochemical impedance experiments. The use of an external reference electrode is unsuitable for these types of experiments with the current setup and cell design.

The electrolyte resistance can be estimated by placing the reference electrode between the working and counter electrodes and assuming that the current passing over the reference electrode does not significantly affect the measurement. Table 6 shows the different estimated resistances based on impedance experiments for the various electrode setups. The different electrode setups are indicated in Figures 36 to 40. The data from table 6 is plotted in Figure 41, showing the electrolyte resistance as a function of distance between the centers of the electrodes.

Table 6. The table shows measured resistance for two different MFFC designs using several electrode setups.

Electrode setup nr.	Electrode setup	Resistance from impedance [Ω]
7	 <p data-bbox="391 653 542 688">Figure 36.*</p>	$8.7 \cdot 10^2$
8	 <p data-bbox="391 951 542 987">Figure 37.*</p>	$2.0 \cdot 10^3$
9	 <p data-bbox="391 1228 542 1264">Figure 38.*</p>	$8.8 \cdot 10^2$
10	 <p data-bbox="391 1505 542 1541">Figure 39.*</p>	$6.7 \cdot 10^3$
11	 <p data-bbox="391 1782 542 1818">Figure 40.*</p>	$5.7 \cdot 10^3$

*Electrode setup for MFFC corresponding to impedance measurement.

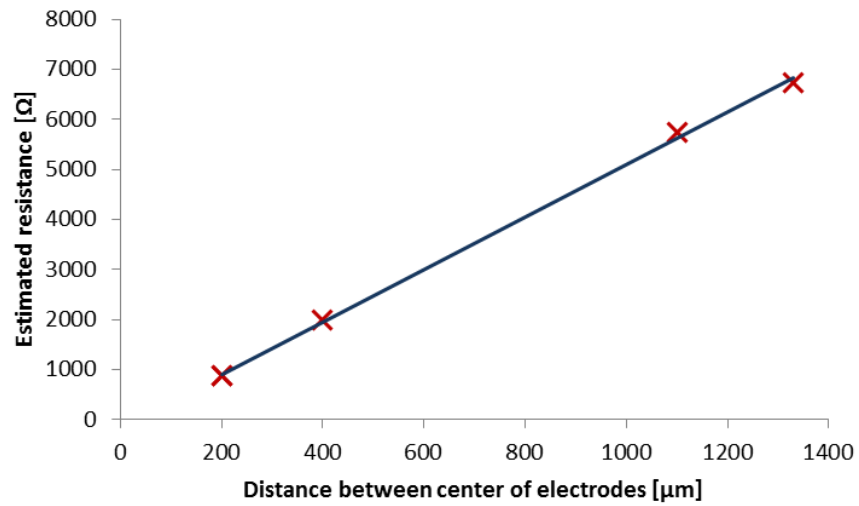


Figure 41. Resistance results from Table 6 plotted as a function of distance between centers of the electrodes.

Electrode setups 7 and 9 yielded comparable results as expected from previous comparison between electrode setups 1 and 3. The results from both cells follow a linear trend. The linear trend is what is expected if one uses a simplified model treating the channel as a material with homogenous conductivity.

4.8 Potentiostatic electrochemical impedance

To better the understanding of the cells electrochemical properties during flow, a series of potentiostatic electrochemical impedance experiments was carried out it proved difficult to achieve reproducibility due to the previously described drift of the open-circuit potential.

Due to the low reproducibility, the results are only evaluated qualitatively. Further work is necessary to solve the problems with drift of the open-circuit potential and establish the conditions required for better reproducibility.

Figure 42 shows a sample of results at different flow rates using electrode setup 4 with the reference electrode placed upstream from the working and counter electrodes. The results were collected with an internal reference and the ruthenium redox couple.

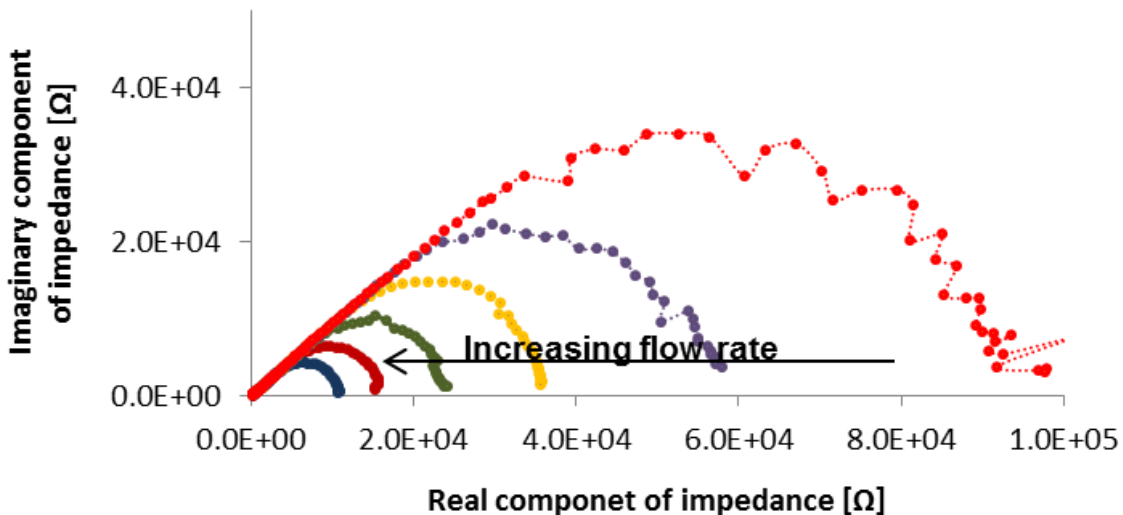


Figure 42. Measured potentiostatic impedance for five different for flow rates in MFFC.

At high frequencies we see a straight line at 45°. This indicates diffusion controlled process with no limit in diffusion layer thickness and is well established by the Warburg impedance. Then the impedance is influenced by the flow rate and this limits the diffusion layer thickness until a pure phase diffusion process is visible at very low

frequencies measuring a pure diffusion through a constant layer. A higher flow rate reduces this thickness and makes the flux across the layer higher. This gives a higher current at the same potential reducing the resistance. These trends can be observed in Figure 42.

4.9 Downstream galvanostatic electrochemical impedance

Using galvanostatic impedance and attaching the working sense electrode downstream of the working electrode, it is possible to collect data in a 4-electrode mode. This configuration allows a downstream detection scheme with a regular potentiostat that would otherwise require a bi-potentiostat. This gives a setup similar to the collection efficiency measurement described in Chapter 2.1.1. The only difference is that the collector electrode measures the potential at a controlled current and not the current at a controlled potential.

The ruthenium redox couple is a fast and reversible reaction. This allows for the simplification that the Nernst equation is valid at the electrode surface at all times. The solution used contained equal parts of each ruthenium complex. Using the Nernst equation the measured potential can be converted into a concentration difference relative to the starting concentration. The measured potential relative to the upstream reference electrode oscillates in phase with the concentration oscillation at the sense (collector) electrode, and its amplitude is proportional to the concentration amplitude there.

The oscillations are generated at the working (generator) electrode where current generates a sine wave concentration profile at the applied frequency. When this signal reaches the collector it is phase shifted due to its travel time down the channel and diffusion into the channel. At low frequencies the period of a cycle is much larger than the transport time down the channel due to convective flow of the fluid. Therefore the collector electrode changes can “keep up” with the changes at the generator electrode. The consequence of this is that both of the electrodes are in phase. The difference in concentration amplitude at the two electrodes can mainly be contributed to diffusion in to the channel which reduces the collection efficiency.

As the frequency increases the two electrodes becomes phase shifted. This gives rise to an imaginary part of the impedance. In the simplest approximation where the amplitude

of the concentration does not decrease down the channel (100% collection efficiency) and the effect propagates down the channel with the average fluid velocity, the phase ($\rho = \omega d v^{-1}$) will depend only on the distance (d), velocity (v) and frequency (ω). Since the amplitude is constant, and the phase increases with frequency, the Nyquist impedance should be a circle.

The signal will weaken due to diffusion in to the channel during the transport time between the electrodes. This effect combined with the phase shift causes the Nyquist-plot to spiral inwards. This effect clearly visible in Figure 43. The dependence of flow rate on the magnitude of the impedance is similar to the potentiostatic impedance experiment. The figure shows similarly features as Figure 42. Both results follow the general trend that higher flow rate decreases the magnitude of the impedance.

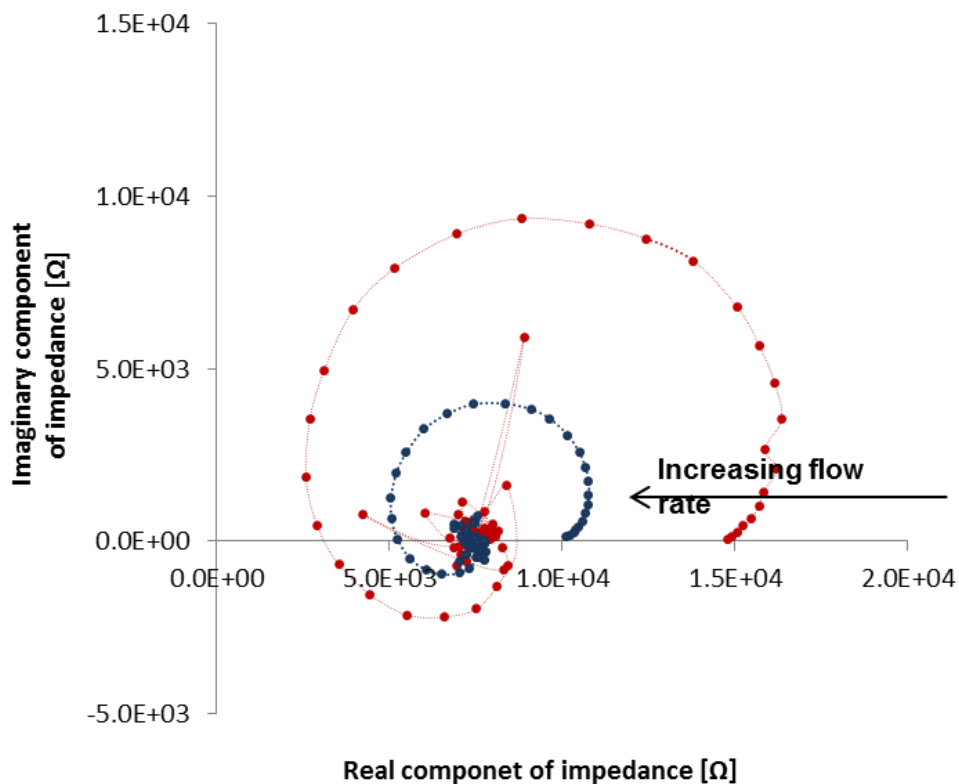


Figure 43. Measured downstream-galvanostatic impedance for two different for flow rates in MFFC.

The simple analysis assumes that there are unique phases at the generator and collector electrodes. This is only true if the width of the electrodes is small compared to the wavelength of the concentration waves. The electrodes used in the MFFCs are 100 μm wide. This in combination with the low flow rate of the bulk electrolyte causes the concentration waves to be shorter than width of the electrodes for frequency higher than 100 Hz for most applicable flow rates. This effect is assumed to cause the chaotic behavior at the center of the circle.

Using cell design B and electrode 4 it should be possible to record several 360° turns for the spiral. However the large distance results in longer travel times causing diffusion to reduce magnitude of the concentration profile resulting in small signal to noise ratio making this assumption difficult to verify.

5. Conclusion

Two changes to the previously established manufacturing techniques for the production of MFFCs were implemented. Changing the template for PDMS-masters from square glass-slides to circular silicon wafer increased the lifetime master and the improved the quality and control over the channel parameters. Replacing three-layer electrodes consisting of titanium, gold and platinum with two-layer electrodes consisting of titanium and platinum slowed down the degradation of the electrodes and provided electrodes with a known surface composition. The three-layer electrodes showed exposed gold surface both using a light microscope and during electrochemical experiments.

A method for removal of oxygen from the MFFCs was established using argon purged solutions and a custom made environmental chamber. Oxygen proved difficult to remove probably due to oxygen leaking out from the PDMS creating a flow of oxygen until the PDMS was depleted.

The ferro/ferricyanide redox couple showed irreversible behavior in MFFCs. In order to achieve ideal behavior the platinum surface was covered with a layer of iodine. This did not improve the reversibility of the redox couple significantly. The irreversibility of the redox couple is probably caused by Prussian blue deposits on the surface inhibiting electron transfer.

The ruthenium (II/III) redox couple showed close to ideal reversible behavior both with and without the iodine layer. The iodine layer inhibited secondary reaction at low potential and prevented the buildup of surface species. The increased stability and the ability to prevent the buildup of surface species resulted in the implementation of iodine-layer platinum electrodes with the ruthenium redox as a part of the standardized experimental setup.

The placement of the reference electrode in the MFFCs showed a significant effect on the measurements. The general trend is that the reference electrode should be situated

as close as possible up-stream for the working electrode and the distance of counter electrode down-stream for the working electrode should exceeded the distance the distance between the working and reference electrode to minimize interference.

Results from potentiostatic electrochemical impedance were qualitatively evaluated and found consistent trends presented in the literature. The magnitude of the impedance decreased with increasing flow rate consistent with expectation. The results were not evaluated quantitatively due to fluctuating open-circuit potential influencing the reproducibility.

Results from downstream impedance suffered from the same lack of reproducibility due to the fluctuating open-circuit potential. These results showed an inward spiral in the Nyquist plot. The spiraling motion was caused by the shift in phase between the generator and collector electrode and the inward motion was a result of diffusion in to the channel during the transportation time of the fluid.

Significant advances were made to both the production and electrochemical characterization of the MFFCs. Although the use of MFFCs for study of electrochemical reactions is in its infancy the results in this work shows great promises for future work.

6. Further work

Further work should be divided in to three different parts; improvements to the manufacturing procedure and design of MFFCs, further electrochemical characterization of MFFCs and the use of MFFCs for electrochemical studies of small organic molecules.

Manufacturing procedure and design for MFFCs

The biggest weakness with the current procedure for manufacturing MFFCs is the problems with manufacturing electrodes in the sub 50 μm scales. Scaling down the cells or some electrodes can be of interest in exploring new techniques or trying to emulate the infinite thin electrodes used for the simple approximation for the downstream impedance.

Electrochemical characterization of MFFCs

Problems with the fluctuating open-circuit potential must be solved in order to achieve reproducible results. Efforts should be made in order to figure out the cause of this problem and stabilizing the open-circuit potential. Once the cells produce reproducible results, the results should be studied and evaluated against theoretical models to better the understanding of the system. Data-simulation can be a useful tool to link the empirical data obtained during the characterization with available theoretical models.

Electrochemical studies of simple organic fuels

The MFFCs were created for the purpose of studying the electrochemical oxidation of small organic fuels. Further work should therefore include extensive studies on fuels such as formic acid, methanol and ethanol to better the understanding of their electrochemical pathways and kinetic parameters to assist the development of suitable electrocatalysts.

7. References

- [1] D.H. Seland Frode, Svein Sunde, in, 2012.
- [2] T.R.L.C. Paixao, R.C. Matos, M. Bertotti, *Electrochim Acta*, 48 (2003) 691-698.
- [3] D. Daniel, I.G.R. Gutz, *Talanta*, 68 (2005) 429-436.
- [4] P. Forsberg, E.O. Jorge, L. Nyholm, F. Nikolajeff, M. Karlsson, *Diam Relat Mater*, 20 (2011) 1121-1124.
- [5] E. Kjeang, N. Djilali, D. Sinton, *J Power Sources*, 186 (2009) 353-369.
- [6] S.A.M. Shaegh, N.T. Nguyen, S.H. Chan, *Int J Hydrogen Energ*, 36 (2011) 5675-5694.
- [7] N. Triroj, P. Jaroenapibal, R. Beresford, *Sensor Actuat B-Chem*, 187 (2013) 455-460.
- [8] E. Kjeang, B. Roesch, J. McKechnie, D.A. Harrington, N. Djilali, D. Sinton, *Microfluid Nanofluid*, 3 (2007) 403-416.
- [9] H. Rajantie, J. Strutwolf, D.E. Williams, *J Electroanal Chem*, 500 (2001) 108-120.
- [10] E. Bitziou, M.E. Snowden, M.B. Joseph, S.J. Leigh, J.A. Covington, J.V. Macpherson, P.R. Unwin, *J Electroanal Chem*, 692 (2013) 72-79.
- [11] H. Mizuguchi, K. Shibuya, A. Fuse, T. Hamada, M. Iiyama, K. Tachibana, T. Nishina, J. Shida, *Talanta*, 96 (2012) 168-173.
- [12] I.B. Svir, A.I. Oleinick, R.G. Compton, *J Electroanal Chem*, 560 (2003) 117-126.
- [13] E. Kjeang, B.T. Proctor, A.G. Brolo, D.A. Harrington, N. Djilali, D. Sinton, *Electrochim Acta*, 52 (2007) 4942-4946.
- [14] C.H. Hamann, A. Hamnett, W. Vielstich, *Electrochemistry*, Wiley -VCH, Weinheim ; New York, 1998.
- [15] D.A. Harrington, in, University of Victoria, 2004.
- [16] C. Beriet, D. Pletcher, *J Electroanal Chem*, 361 (1993) 93-101.
- [17] J. Kawiak, P.J. Kulesza, Z. Galus *J Electroanal Chem*. 226 (1987) 305-314.
- [18] K. Itaya, T. Ataka, S. Toshima, *J Am Chem Soc*, 104 (1982) 4767-4772.
- [19] I. Streeter et.al., *J. Phys. Chem C* (2007), 111, 12058-12066.
- [20] M. Muzokár, W.R. Fawcett, *Anal Chem* (2004), 76, 3607-3611.
- [21] P.S. Bagus, C Wöll, A Wieckowski, *Surface Science* (2009), 273-283.
- [22] A.E. Thomas, A. Wieckowski *J Electroanal Chem*. 399 (1995) 207-212.
- [23] S. Swarthirajan, S. Bruckenstein, *J Electroanal Chem*. 125 (1981) 63-71.
- [24] L.M. Dané et.al., *Electrochimica Acta* (1968) Vol. 13 pp. 507 to 518.
- [25] M. Quirk, J. Serda, *Semiconductor manufacturing technology*, Prentice Hall, Upper Saddle River, NJ, 2001.
- [26] X. Li, N.Q. Wu, Y. Rojanasakul, Y.X. Liu, *Sensor Actuat a-Phys*, 193 (2013) 186-192.
- [27] J.C. McDonald, D.C. Duffy, J.R. Anderson, D.T. Chiu, H.K. Wu, O.J.A. Schueller, G.M. Whitesides, *Electrophoresis*, 21 (2000) 27-40.
- [28] C. Møinichen, in: Department of Materials Science and Engineering, NTNU, Trondheim, 2012.
- [29] M. Ingdal, in: Department of Materials Science and Engineering, NTNU, Trondheim, 2013.
- [30] *MicroCHEM* (2014) PROCESSING GUIDELINES FOR:SU-8 2100 and SU-8 2150.
- [31] S.E.C Dalé et.al, *Electrochimica Acta* (2014) Vol. 126 pp. 94 to 100

Appendix A

Detailed step-by-step procedure for production of MFFCs.

Procedure for production of electrodes

All work with production of electrodes was performed in ISO 5+6 certified cleanroom. All work with undeveloped photoresist was done in an area with UV-filtered light.

Cleaning and dehydration bake

Glass slides were cut into pieces (approximately 2.5 cm x 3.5 cm) using a scribe and cleaned in acetone using an ultrasonic bath (5 min., medium intensity). Glass slides were thereafter dried using nitrogen gas. The same procedure was repeated using isopropanol instead of acetone. After the drying step the glass slides were cleaned using a plasma-cleaner (10 min., 50 % O₂, 50 W). The clean glass slides were then dehydration baked using a heating oven (10 min, 200 °C).

Spin coating and soft bake

After the dehydration bake, photoresist (ma-405) was applied using spin coating (30 sec., 1000 rpm, 250 rpm s⁻¹). The glass slides were held in place using vacuum, and the entire surface of the glass slides were covered in photoresist prior to spinning. After the spin coating, the glass slides were soft baked using a hotplate (60 sec., 100 °C). Figure 13 shows an illustration of a glass slide covered in photoresist after soft bake.

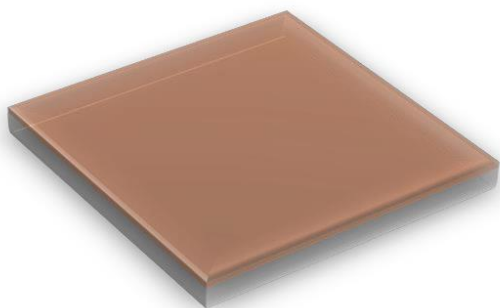


Figure 13. Illustration of a glass slide after completing spin coating and soft baking-step of the manufacturing procedure.

Exposure and alignment

After soft-baking, the glass slides were exposed to UV-light using a mask aligner. The exposure time was determined by measuring the intensity of the UV-source, and calculating the necessary time to reach desired exposure-dose (400 mJ cm^{-2}). The mask was cleaned using ethanol and inserted into the mask aligner in such a way that the desired pattern was centered in the mask holder. The glass slides were placed into the mask aligner on top of a SOLARONIX UV filter. The glass slides were then moved so the desired pattern of the mask was centered. The glass slides were exposed using hard contact between the mask and sample. Figure 14 shows an illustration of the glass slide after exposure.

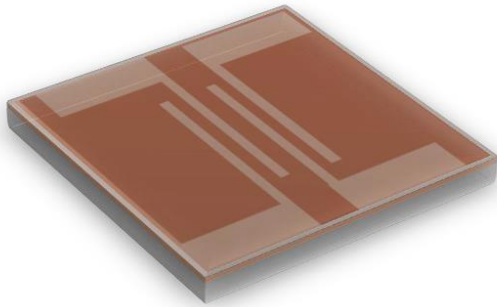


Figure 14. Illustration of a glass slide after completing exposure and alignment-step of the manufacturing procedure.

Development

After exposure, the glass slides were developed using a developer (ma-D331/s). The glass slides were developed for approximately 150 sec. until no thin film could be observed on the unexposed areas. After development the samples were immediately rinsed in water and dried using nitrogen gas. Figure 15 shows an illustration of a glass slide with developed photoresist with the electrode negative pattern.

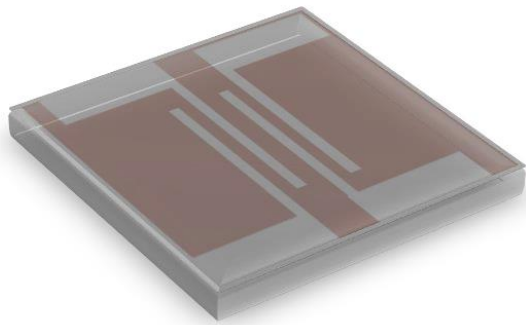


Figure 15. Illustration of a glass slide after completing the development-step of the manufacturing procedure.

Metal deposition

Before metal deposition the developed glass slides were cleaned using a plasma-cleaner (10 min, 50 % O₂ 50 W). The glass slides were then mounted on to a silicon wafer (4") using double sided tape and inserted into the e-beam evaporator. Different combinations of metals and thicknesses were used for electrode composition, but all included an initial layer of titanium (10 nm) to secure adhesion to the glass surface. Metal was deposited at the surface in the desired combination, and the glass slides were removed from the evaporation chamber. Figure 16 shows an illustration of a glass slide straight out of the e-beam evaporator covered in metal.



Figure 16. Illustration of a glass slide after completing the metal deposition-step of the manufacturing procedure.

Lift-off

Excess metal was removed using lift-off. The glass slides were emerged in photoresist remover solution (mr-REM-660) until the pattern was clean and clearly visible. A brush was often used to speed up the process. After the electrode pattern was clean and fully visible the glass slides were removed from the solution and cleaned in water and dried using nitrogen gas. Figure 17 shows an illustration of a glass slide including electrodes after lift-off.

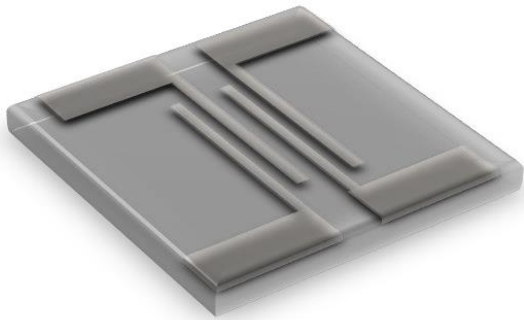


Figure 17. A illustration of a glass slide after completing the lift-off-step of the manufacturing procedure.

Inspection

The electrodes were then inspected in a light microscope, for possible damages and short circuits. For larger electrodes this can be done without a microscope. A multimeter was used to control the individual resistant for each electrode between the base and tip of the electrodes and to ensure no short circuits. Figure 18 shows a picture using a light microscope during electrode inspection.

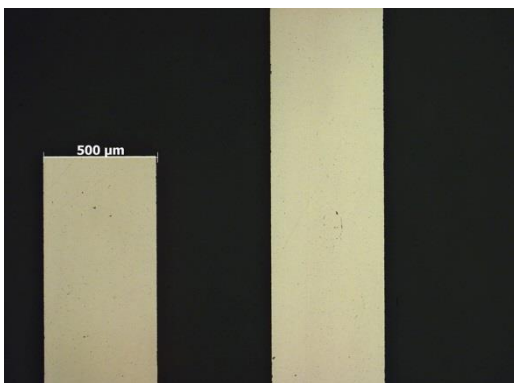


Figure 18. A picture of the electrodes using a light microscope during inspection.

Procedure for the production of PDMS-masters

All work with production of PDMS-masters was performed in ISO 5+6 certified cleanroom. All work with undeveloped photoresist was done in an area with UV-filtered light.

Cleaning and dehydration bake

Silicon wafers (D = 2", t = 1 mm) were cleaned the same manner as "the production of electrodes" up to and including dehydration bake.

Spin coating and soft bake of main layer

A thick layer of photoresist (SU-8 2100) was then applied on top of silicon wafer. The wafer were held in place with a vacuum and the photoresist was smeared on top of the wafer, trying to cover the entire surface in an even manner and avoiding air bubbles. The wafer were then spun in a two-step process (Step1: 500 rpm, 10 sec., 500 rpm s⁻¹, Step2: 3000 rpm, 30 sec, 300 rpm s⁻¹). After the spin coating the glass wafer were baked in a two-step process (Step 1: 5 min., 65 °C, Step 2: 25 min., 95 °C) and cooled to room temperature.

Alignment and exposure

After the wafers had cooled to room temperature they were ready for exposure. The exposure time was determined by measuring the intensity of the UV-source, and calculating the necessary time to reach desired exposure-dose (200 mJ cm⁻²). The mask was cleaned with ethanol and the desired channel pattern was chosen, inserted and centered in the mask aligner. The alignment was used to avoid air bubbles and other irregularities in the photoresist surface. The wafers were exposed using proximity between the mask and sample to avoid the photoresist sticking to mask.

Post exposure bake

After exposure the wafers were hard baked using a two-step process (Step 1: 5 min., 65 °C, Step 2: 11 min., 95 °C) and cooled to room temperature.

Development

The wafers were then then developed using a developer (mr-Dev 600) until the photoresist pattern was clearly visible (approximately 10-20 min). The wafers were immediately rinsed in water and dried using nitrogen gas.

Hard bake

After development the wafers were hard baked (150°C, 15 min.) and cooled to room temperature.

Inspection

A profilometer was used to determine the profile of the negative channel and give a visual inspection at a microscopic level. The PDMS-masters was marked with a letter corresponding to their profilometer measurements.

Procedure for production of PDMS-channels

All work with production of PDMS-channels was performed in ISO 7 certified cleanroom. All work with uncured PDMS was performed in a dedicated fume hood to avoid contamination.

Mixing and curing

Silicon elastomer base (25 g) was mixed with a silicon elastomer curing agent (2 g) in a plastic cup and stirred. The cup with the mixture was then degassed in a vacuum (15 min.). Some of the degassed mixture was thereafter poured in to a plastic dish so that the bottom of the dish was covered. The PDMS-masters were then placed in the dish with the channel side up and then covered with the rest of the mixture. The dish was then degassed in a vacuum until no bubbles could be observed (30 min). After the degassing the dish was moved to a heating oven and left there until the curing process was completed (40 min, 80 °C).

Cutting and customization

The cured PDMS was cut into a slab containing one channel using a scalpel. The PDMS-slab was cut into an appropriate size for fitting on top of the electrodes without covering the whole glass slide. Two holes were made, one for the tube ($D = 0.5$ mm) and one for the reservoir ($D = 2$ mm). The hole made for the tube was angled in such a way that the entrance of the tube would be at the short end of the PDMS-slab. The hole made for the reservoir was vertical, exiting on the top of the PDMS-slab.

Assembly of MFFC

Mounting of the PDMS channels to the electrode surface was performed in ISO 7 certified cleanroom. All other assembly work was done outside the clean room.

Mounting of PDMS channel

Before mounting the PDMS channel to electrode surface, the surfaces of PDMS-slab was activated and the electrode side cleaned. Activation and cleaning was done using the plasma cleaner (24 s, 100% O₂, 20 W) on the channel side of the PDMS-slab and electrode side of the glass slide. After activation the active side of the PDMS-slab was centered and placed on top of the electrode side of the glass slide constituting the main part of MFFC. The MFFC was then placed inside a heating cabinet to enhance the adhesion between the two parts (40 min, 80 °C).

Mounting of reservoir and plastic tubing

The MFFC was thereafter removed from the clean room. A glass cylinder ($D = 14$ mm, $h = 20$ mm) was used for a reservoir. The reservoir was mounted on top of the PDMS using silicon glue, making sure that the hole intended for the reservoir was not covered but exits inside the glass cylinder. Additional silicon glue was used to prevent leakage for the reservoir. Plastic tubing (1.0 mm) was forced into the last remaining hole at the short end of the PDMS-slab. Silicon glue was used to fasten the plastic tube and prevent leakage.

Attachment of wires and control of electrical connections

Electric wires was stripped at both ends, marked with the numbers 1-4 and fastened to their respective electrode (Electrode 1 is the electrode closest to the plastic tubing and 4 is the electrode closest to the reservoir). The wires were soldered to the electrode surface using a soldering iron. A multimeter was used to control for short circuits and the conductive contention between the end of the wire and the electrode surface.